ular chaperone and intracellular Ca^{2+} regulator [29,30]. Several previous reports have shown that gp96 is glycosylated and phosphorylated, and exists as heterogeneous molecular entities with various molecular weights [31]. In order to know whether gp96 spots were phosphorylated or not, we stained the 2-DE gels with ProQ Diamond which is a dye specific to proteins phosphorylated on serine, threonine or tyrosine residues [32], and has been used successfully to visualize phosphoproteins [33]. We found that the spot #436 was positively stained with ProQ (Fig. 3E and F). We further tried to detect possible phosphorylated peptides in the tryptic digests prepared from #436 by MALDI–TOF–MS according to Nabetani et al. [21]. Searching for those peaks that had relatively stronger intensities in negative ion mode than in positive ion mode, we found two peaks as candidates for acidically modified peptides. They were assigned to the peptides SILFVPT-SAPR (amino acid sequence: 385–395, data not shown) and FQSSHHPTDITSLDQYVER (aa512–530). Fig. 3G and H show the unmodified peak and the acidically modified peak (mass shifted by +80 Da in negative ion mode) of the latter peptide, respectively. This peptide contained a predicted phosphorylation consensus motif, [Ser or Thr]-X-X-[Asp or Glu], for protein kinase CK2 (Fig. 3G) which was suggested to phosphorylate gp96 [34]. These results together with ProQ staining indicated that at least one gp96 isoform was phosphorylated and was up-regulated in HCC. Over-expression of gp96 in HCC has been reported previously [35], though the reports that showed over-expression of its phosphorylated form are rare. Further investigation into biological meaning of gp96 phosphorylation may provide us important information about HCC development.

Acknowledgments

Appendix A. Supplementary data

Supplementary data associated with this article can be found, in the online version, at doi:10.1016/j.bbrc.2007.11.101.

References

[1] T.K. Seow, R.C.M.Y. Liang, C.K. Leow, M.C.M. Chung, Hepatocellular carcinoma: from bedside to proteomics, Proteomics 1 (2001) 1249–1263.

[2] L.J. Lopez, J.A. Marrero, Hepatocellular carcinoma, Curr. Opin. Gastroenterol. 3 (2004) 248–253.

[3] H.F. Kawai, S. Kaneko, M. Honda, Y. Shirota, K. Kobayashi, Alpha-fetoprotein-producing hepatoma cell lines share common expression profiles of genes in various categories demonstrated by cDNA microarray analysis, Hepatology 3 (2001) 676–691.

[4] N. Iizuka, M. Oka, H. Yamada-Okabe, N. Mori, T. Tamesa, T. Okada, N. Takemoto, K. Hashimoto, et al., Differential gene

[5] T. Yamashita, S. Kaneko, S. Hashimoto, T. Sato, S. Nagai, N. Toyoda, T. Suzuki, K. Kobayashi, et al., Serial analysis of gene expression in chronic hepatitis C and hepatocellular carcinoma, Biochem. Biophys. Res. Commun. 282 (2001) 647–654.

[6] K. Kawaguchi, M. Honda, T. Yamashita, Y. Shirota, S. Kaneko, Differential gene alteration among hepatoma cell lines demonstrated by cDNA microarray-based comparative genomic hybridization, Biochem. Biophys. Res. Commun. 329 (2005) 370–380.

[7] Y. Midorikawa, M. Makuuchi, W. Tang, H. Aburatani, Microarray-based analysis for hepatocellular carcinoma: from gene expression profiling to new challenges, World J. Gastroenterol. 13 (2007) 1487–1492.

[8] N.A. Shackel, D. Seth, P.S. Haber, M.D. Gorrell, G.W. McCaughan, The hepatic transcriptome in human liver disease, Comp. Hepatol. 5 (6) (2006).

[9] T.J. Griffin, S.P. Gygi, T. Ideker, B. Rist, J. Eng, L. Hood, R. Aebersold, Complementary profiling of gene expression at the transcriptome and proteome levels in Saccharomyces cerevisiae, Mol. Cell. Proteomics 4 (2002) 323–333.

[10] S.P. Gygi, Y. Rochon, B.R. Franza, R. Aebersold, Correlation between protein and mRNA abundance in yeast, Mol. Cell. Biol. 19 (1999) 1720–1730.

[11] M. Unlu, M.E. Morgan, J.S. Minden, Difference gel electrophoresis: a single gel method for detecting changes in protein extracts, Electrophoresis 11 (1997) 2071–2077.

[12] I.N. Lee, C.H. Chen, J.C. Sheu, H.S. Lee, G.T. Huang, C.Y. Yu, F.J. Lu, L.P. Chow, Identification of human hepatocellular carcinoma-related biomarkers by two-dimensional difference gel electrophoresis and mass spectrometry, J. Proteome Res. 6 (2005) 2062–2069.

[13] C.R. Liang, C.K. Leow, J.C. Neo, G.S. Tan, S.L. Lo, J.W. Lim, T.K. Seow, P.B. Lai, et al., Proteome analysis of human hepatocellular carcinoma tissues by two-dimensional difference gel electrophoresis and mass spectrometry, Proteomics 5 (2005) 2258–2271.

[14] V.J. Desmet, M. Gerber, J.H. Hoofnagle, M. Manns, P.J. Scheuer, Classification of chronic hepatitis: diagnosis, grading and staging, Hepatology 19 (1994) 1513–1520.

[15] K.G. Ishak, P.P. Anthony, L.H. Sobin, Histological typing of tumours of the liver, 2nd ed.WHO International Histological Classification of Tumors, Springer-Verlag, New York, 1994.

[16] M. Honda, S. Kaneko, H. Kawai, Y. Shirota, K. Kobayashi, Differential gene expression between chronic hepatitis B and C hepatic lesion, Gastroenterology 120 (2001) 955–966.

[17] H.F. Kawai, S. Kaneko, M. Honda, Y. Shirota, K. Kobayashi, Alpha-fetoprotein-producing hepatoma cell lines share common expression profiles of genes in various categories demonstrated by cDNA microarray analysis, Hepatology 33 (2001) 676–691.

[18] M. Honda, H. Kawai, Y. Shirota, T. Yamashita, T. Takamura, S. Kaneko, cDNA microarray analysis of autoimmune hepatitis, primary biliary cirrhosis and consecutive disease manifestation, J. Autoimmun. 25 (2005) 133–140.

[19] M. Honda, T. Yamashita, T. Ueda, H. Takatori, R. Nishino, S. Kaneko, Different signaling pathways in the livers of patients with chronic hepatitis B or chronic hepatitis C, Hepatology 44 (2006) 1122–1138.

[20] Y. Tabuse, T. Nabetani, A. Tsugita, Proteomic analysis of protein expression profiles during Caenorhabditis elegans development using 2D-difference gel electrophores, Proteomics 5 (2005) 2876–2891.

[21] T. Nabetani, K. Miyazaki, Y. Tabuse, A. Tsugita, Analysis of acidic peptides with a matrix-assisted laser desorption/ionization mass spectrometry using positive and negative ion modes with additive monoammonium phosphate, Proteomics 6 (2006) 4456–4465.

[22] Y. Kuramitsu, T. Harada, M. Takashima, Y. Yokoyama, I. Hidaka, N. Iizuka, T. Toda, M. Fujimoto, et al., Increased expression and phosphorylation of liver glutamine synthetase in well-differentiated

hepatocellular carcinoma tissues from patients infected with hepatitis C virus, Electrophoresis 27 (2006) 1651–1658.

[23] L. Hu, S.H. Lau, C.H. Tzang, J.M. Wen, W. Wang, D. Xie, M. Huang, Y. Wang, et al., Association of Vimentin overexpression and hepatocellular carcinoma metastasis, Oncogene 23 (2004) 298–302.

[24] Z. Dai, Y.K. Liu, J.F. Cui, H.L. Shen, J. Chen, R.X. Sun, Y. Zhang, X.W. Zhou, Identification and analysis of altered alpha1,6-fucosy-lated glycoproteins associated with hepatocellular carcinoma metastasis, Proteomics 6 (2006) 5857–5867.

[25] E. Zeindl-Eberhart, S. Haraida, S. Liebmann, P.R. Jungblut, S. Lamer, D. Mayer, G. Jäger, S. Chung, H.M. Rabes, Detection and identification of tumor-associated protein variants in human hepato-cellular carcinomas, Hepatology 39 (2004) 540–549.

[26] W.H. Kuo, W.L. Chiang, S.F. Yang, K.T. Yeh, C.M. Yeh, Y.S. Hsieh, S.C. Chu, The differential expression of cytosolic carbonic anhydrase in human hepatocellular carcinoma, Life Sci. 73 (2003) 2211–2223.

[27] P.N. Cheng, T.L. Lam, W.M. Lam, S.M. Tsui, A.W. Cheng, W.H. Lo, Y.C. Leung, Pegylated recombinant human arginase (rhArg-peg5,000mw) inhibits the in vitro and in vivo proliferation of human hepatocellular carcinoma through arginine depletion, Cancer Res. 67 (2007) 309–317.

[28] F.S. Berven, O.A. Karisen, J.C. Murrell, H.B. Jensen, Multiple polypeptide forms observed in two-dimensional gels of Methylococ-cus capsulatus (Bath) polypeptides are generated during the separa-tion procedure, Electrophoresis 24 (2003) 757–761.

[29] J. Melnick, S. Aviel, Y. Argon, The endoplasmic reticulum stress protein GRP94, in addition to BiP, associates with unassembled immunoglobulin chains, J. Biol. Chem. 267 (1992) 21303–21306.

[30] H. Liu, E. Miller, B. van de Water, J.L. Stevens, Endoplasmic reticulum stress proteins block oxidant-induced Ca^{2+} increases and cell death, J. Biol. Chem. 273 (1998) 12858–12862.

[31] A.M. Feldweg, P.K. Srivastava, Molecular heterogeneity of tumor rejection antigen/heat shock protein GP96, Int. J. Cancer 63 (1995) 310–314.

[32] T.H. Steinberg, B.J. Agnew, K.R. Gee, W.-Y. Leung, T. Goodman, B. Schulenberg, J. Hendrickson, J.M. Beechem, R.P. Haugland, W.F. Patton, Global quantitative phosphoprotein analysis using multi-plexed proteomics technology, Proteomics 3 (2003) 1128–1144.

[33] B.R. Chitteti, Z. Peng, Proteome and phosphoproteome dynamic change during cell dedifferentiation in Arabidopsis, Proteomics 7 (2007) 1473–1500.

[34] S.E. Cala, GRP94 hyperglycosylation and phosphorylation in Sf21 cells, Biochim. Biophys. Acta 1496 (2000) 296–310.

[35] D.F. Yao, X.H. Wu, X.Q. Su, M. Yao, W. Wu, L.W. Qiu, L. Zou, X.Y. Meng, Abnormal expression of HSP gp96 associated with HBV replication in human hepatocellular carcinoma, Hepatobiliary Pan-creat. Dis. Int. 5 (2006) 381–386.

Lipid-Induced Oxidative Stress Causes Steatohepatitis in Mice Fed an Atherogenic Diet

Naoto Matsuzawa,[1,2] Toshinari Takamura,[1] Seiichiro Kurita,[1] Hirofumi Misu,[1] Tsuguhito Ota,[1] Hitoshi Ando,[1]
Masayoshi Yokoyama,[1] Masao Honda,[1] Yoh Zen,[3] Yasuni Nakanuma,[3] Ken-ichi Miyamoto,[2] and Shuichi Kaneko[1]

Recently, nonalcoholic steatohepatitis (NASH) was found to be correlated with cardio-
vascular disease events independently of the metabolic syndrome. The aim of this study
was to investigate whether an atherogenic (Ath) diet induces the pathology of steato-
hepatitis necessary for the diagnosis of human NASH and how cholesterol and triglyc-
eride alter the hepatic gene expression profiles responsible for oxidative stress. We
investigated the liver pathology and plasma and hepatic lipids of mice fed the Ath diet.
The hepatic gene expression profile was examined with microarrays and real-time poly-
merase chain reactions. The Ath diet induced dyslipidemia, lipid peroxidation, and
stellate cell activation in the liver and finally caused precirrhotic steatohepatitis after 24
weeks. Cellular ballooning, a necessary histological feature defining human NASH, was
observed in contrast to existing animal models. The addition of a high-fat component to
the Ath diet caused hepatic insulin resistance and further accelerated the pathology of
steatohepatitis. A global gene expression analysis revealed that the Ath diet up-regulated
the hepatic expression levels of genes for fatty acid synthesis, oxidative stress, inflam-
mation, and fibrogenesis, which were further accelerated by the addition of a high-fat
component. Conversely, the high-fat component down-regulated the hepatic gene ex-
pression of antioxidant enzymes and might have increased oxidative stress. *Conclusion:*
The Ath diet induces oxidative stress and steatohepatitis with cellular ballooning. The
high-fat component induces insulin resistance, down-regulates genes for antioxidant
enzymes, and further aggravates the steatohepatitis. This model suggests the critical role
of lipids in causing oxidative stress and insulin resistance leading to steatohepatitis.
(HEPATOLOGY 2007;46:1392-1403.)

1392

Nonalcoholic fatty liver disease (NAFLD) is currently the most common chronic liver condition in the Western world. Clinical, epidemiological, and biochemical data strongly support the concept that NAFLD is the hepatic manifestation of the metabolic syndrome, the constellation of metabolic abnormalities including obesity, dyslipidemia, and insulin resistance.[1] NAFLD includes not only steatosis (without other injury) but also various degrees of inflammation and fibrosis.[2] Simple steatosis is usually considered benign, but the development of inflammatory changes in the liver [called nonalcoholic steatohepatitis (NASH)] is recognized as a precursor to more severe liver disease and sometimes evolves into cryptogenic cirrhosis.[3] It has been recently proposed that NASH is strongly correlated with cardiovascular disease events independently of the metabolic syndrome.[4] Therefore, further investigations of NASH are required to elucidate the pathogenesis of this process and to develop treatments.

To date, however, studies of NASH have been hampered by the absence of a suitable experimental model. The use of genetic defects or targeted overexpression to produce obesity[5] or impaired hepatic lipid metabolism[6] in rodents has been used as an NAFLD model. Although these genetic manipulations can assess the biological importance of each gene in vivo, they might not reflect the natural etiology of NAFLD in patients and rarely lead to the pathology of NASH. The other models frequently used are based on nutritional manipulations. Natural nutritional models have been described, including the use of a sucrose-rich and fat-rich diet.[7] However, in these models, rodents accumulate minimal fat and develop subtle inflammation of the liver. The methionine- and choline-deficient (MCD) model, which is frequently used to produce more progressive liver pathology, leads to the development of steatosis with lobular inflammation and with perisinusoidal and pericentral fibrosis.[8,9] However, this model lacks lipotrophic factors, insulin resistance,[10] or the cellular ballooning that is observed only with the addition of a high-fat component to the MCD diet.[11]

In this study, we focused on an atherogenic (Ath) diet, which contains cholesterol and cholic acid. Because the diet produces not only an Ath lipoprotein profile but also vascular fatty streak lesions, it has been widely used to study atherosclerosis in animals, including mice.[12] Although the Ath diet has recently been reported to induce liver steatosis, inflammation, and fibrosis,[13] lipid metabolism, insulin resistance, and hepatic gene expression profiles responsible for liver pathology remain to be determined in this model. To address this issue, we investigated the time course of the pathological changes and gene expression profiles of the liver in mice fed the Ath

Table 1. The Composition of the 3 Diets

Composition	Control	Ath	Ath+HF
CRF-1 (%)	100	90.75	38.25
Cocoa butter (%)	–	7.50	60.0
Cholesterol (%)	–	1.25	1.25
Cholate (%)	–	0.50	0.50 (wt/wt %)
Energy composition	Control	Ath	Ath+HF
Carbohydrate (g)	60.9	55.2	23.3
Protein (g)	22.4	20.3	8.6
Fat (g)	6.0	14.0	60.0
Total calorie (kcal)	363	411	669 (/100 g)

The contents of vitamins and minerals in each diet are presented in Supplementary Table 1.

diet. In addition, by adding a high-fat component to the Ath diet, we elucidated the impact of insulin resistance, which is commonly observed in NASH patients, on the development of oxidative stress in the liver and pathology of steatohepatitis.

Materials and Methods

Animals and Experimental Design. Male C57Bl/6J mice were purchased from Charles River Laboratories Japan (Yokohama, Japan) at 6 weeks of age. After 2 weeks of acclimation, the mice were divided into the following 3 groups: (1) control mice given a standard chow (CRF-1, Charles River Laboratories Japan), (2) mice given an Ath diet, and (3) mice fed an atherogenic and high-fat (Ath+HF) diet. The Ath and Ath+HF diets were prepared by the addition of cocoa butter, cholesterol, and cholate to CRF-1. These diets were prepared by Oriental Yeast (Tokyo, Japan). The compositions of each diet are shown in Table 1 and Supplementary Table 1. At 6 weeks of age, the mice were housed in colony cages with a 12-hour light/12-hour dark cycle, and they were given food and water *ad libitum*. All animal procedures were in accordance with the standards set forth in the Guidelines for the Care and Use of Laboratory Animals at the Takara-Machi campus of Kanazawa University (Japan).

Blood Sampling and Analysis. At 6, 12, or 24 weeks, blood samples were obtained from the tail vein following a 12-hour fast. Enzymatic assays for the total cholesterol, free cholesterol, free fatty acids (FFAs), triglyceride (TG), and alanine aminotransferase (ALT) were performed with kits purchased from Wako Pure Chemical Industries (Osaka, Japan). The cholesterol and TG profiles in plasma lipoproteins were analyzed with a dual-detection high-performance liquid chromatography (HPLC) system with 2 tandem connected TSKgel LipopropakXL

columns (300 × 7.8 mm; Tosoh, Japan) by Skylight Biotech (Akita, Japan).[14]

Glucose Tolerance Tests (GTTs) and Insulin Tolerance Tests (ITTs). At 12 weeks, GTTs and ITTs were conducted. For GTTs, glucose was administered (1.5 g/kg body weight) following a 12-hour fast. For ITTs, mice were injected intraperitoneally with insulin (0.5 U/kg of body weight; Humulin R, Eli Lilly, Indianapolis, IN) following a 4-hour fast. The glucose values were measured from whole venous blood with a blood glucose monitoring system (FreeStyle, Kissei, Matsumoto, Japan) 0, 15, 30, 60, and 120 minutes after the administration of glucose or insulin.

Pyruvate Challenge Test. At 6 weeks, we conducted the pyruvate challenge test.[15,16] The mice, deprived of food for 16 hours, were injected intraperitoneally with pyruvate dissolved in saline (2 g/kg). The blood glucose values were measured 0, 15, 30, 60, and 90 minutes after the injection of pyruvate.

Tissue Preparation and Histological Examination. At 6, 12, or 24 weeks, the mice were killed by cervical dislocation under diethyl ether anesthesia following a 12-hour fast. The livers were immediately removed and weighed. A large portion of each liver was snap-frozen in liquid nitrogen for later RNA studies. The remaining tissue was fixed in 10% buffered formalin, processed, and embedded in paraffin for hematoxylin-eosin (H&E), Azan, and Sirius red staining and was blindly scored by a single pathologist. Steatosis, fibrosis, and acinar inflammation were semiquantitatively evaluated according to the standard criteria of grading and staging for NASH, with minor modifications.[17] To evaluate steatosis, we used the absolute percentage of the macrovesicular fat droplet area in the section area (that is, 8 × 10^5 hepatocytes in 4 mm^2). For inflammation, 0 was defined as no hepatocyte injury or inflammation, 1 was defined as mild focal injury, 2 was defined as noticeable injury, and 3 was defined as severe zone 3 hepatocyte injury or inflammation. For fibrosis, 0 was defined as no fibrosis, 1 was defined as pericellular and perivenular fibrosis, 2 was defined as focal bridging fibrosis, 3 was defined as much bridging fibrosis with lobular distortion, and 4 was defined as cirrhosis.

Slides were immunostained with monoclonal mouse anti-human α-smooth muscle actin (α-SMA; Dako Japan, Kyoto, Japan). This was followed by the application of the immunoperoxidase technique with an Envision kit (Dako Japan). The peroxidase activity was identified by a reaction with 3′,3′-diaminobenzidine (Sigma, St Louis, MO). Areas staining for α-SMA were quantified morphometrically with WinROOF version 5.7 (Mitani Shoji,

Fukui, Japan) and expressed as percentages of the field area.

Measuring the Hepatic Lipid Content. Hepatic lipids were extracted with chloroform/methanol (2:1) according to a published method.[18] With a kit (Wako), the extract was dissolved in water and subsequently analyzed for TG, total cholesterol, free cholesterol, and FFAs.

Measuring the Hepatic Hydroxyproline Content. The hydroxyproline content in liver samples was quantified colorimetrically according to a published method.[19] Briefly, a 0.2-g liver sample was homogenized in 6 N HCl and hydrolyzed at 110°C for 16 hours. The hydrolysate was filtered, aliquots were evaporated under a vacuum, and the sediment was redissolved in 50% isopropanol. Then, the samples were incubated in a solution containing 0.84% chloramine-T, 42 mM sodium acetate, 2.6 mM citric acid, and 39.5% (vol/vol) isopropanol (pH 6.0) for 10 minutes at room temperature. Next, the samples were incubated in a solution containing 0.248 g of *p*-dimethylaminobenzaldehyde dissolved in 0.27 mL of 60% perchloric acid and 0.73 mL of isopropanol for 90 minutes at 50°C. The hydroxyproline content was quantified photometrically at 558 nm.

Measuring Hepatic Protein Carbonyls. The concentration of hepatic proteins containing carbonyl groups (those that react with 2,4-dinitrophenylhydrazine to form the corresponding hydrazone) was determined spectrophotometrically according to the instructions with a protein carbonyl assay kit (Cayman Chemical, Ann Arbor, MI).

RNA Preparation for the Microarray Analysis. Total RNA was isolated from the frozen liver with the ToTALLY RNA kit (Applied Biosystems, Foster City, CA). Each sample was prepared by equal amounts of total RNA being pooled from 3 mice in the same group. Three micrograms of total RNA was used to synthesize antisense RNA with the AminoAllyl MessageAmp II antisense RNA kit (Applied Biosystems) for oligo-microarrays (AceGene Mouse Oligo Chip 30K, DNA Chip Research, Yokohama, Japan). Each microarray hybridization sample and the reference amino allyl antisense RNA were labeled with Cy5 and Cy3, respectively. Hybridization and washing were performed according to the manufacturer's instructions; this was followed by scanning with a G2505B microarray scanner (Agilent Technologies, Palo Alto, CA) and then image analysis with GenePix Pro 4.1 software (Axon Instruments, Union City, CA). Microarray data were normalized (LOWESS [locally weighted polynomial regression] method) with GeneSpring version 7.2 software (Agilent Technologies). For the pathway analysis, we used the GenMAPP and MAPPFinder software package.[20,21] The GenMAPP program contains
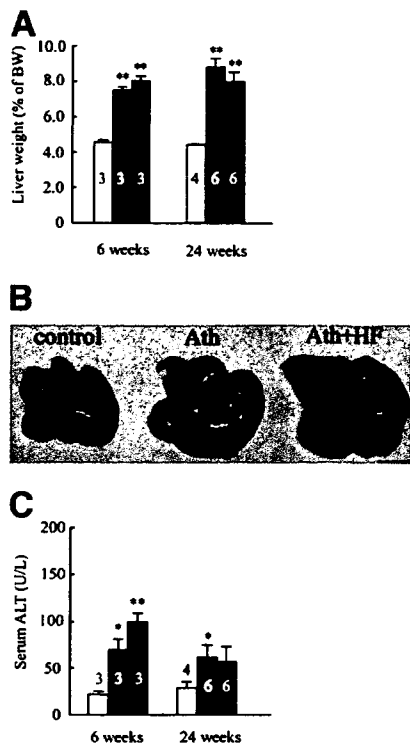
Fig. 1. Effects of 3 diets on the liver weight and morphology and serum ALT. (A) Liver weight with respect to the body weight (BW) of control mice fed standard chow (white bars), the Ath diet (gray bars), or the Ath+HF diet (black bars) after 6 or 24 weeks. (B) Photograph of livers after 12 weeks of feeding with the standard chow, Ath diet, or Ath+HF diet (scale bars: 10 mm). (C) Serum ALT levels after 6 or 24 weeks. The values represent the means ± the SEM. The number of animals per group is indicated in or just above the bars. *P < 0.05 and **P < 0.01 versus the control group.

many pathway maps that can be associated with imported microarray data. The MAPPFinder program, which links gene expression data to the pathway maps, can calculate the z score (standardized difference score) and the percentage of genes measured that meet user-defined criteria (±25% in the change fold in our analysis). With the z score and the percentage, the pathways were ranked according to the relative change in the gene expression. The microarray data sets have been submitted to the Genome Expression Omnibus Database (available at http://www.ncbi.nlm.nih.gov/geo/) under series GSE5852.

Quantitative Real-Time Polymerase Chain Reaction (PCR). The reverse transcription of 100 ng of total RNA (the same sample used for the microarray analysis) was performed with Oligo(dT)$_{12-18}$ primer and Super-Script III reverse transcriptase (Invitrogen, Carlsbad, CA). PCR was performed on an ABI-Prism 7900HT (Applied Biosystems). The specific PCR primers and TaqMan probe used in this study were obtained from Applied Biosystems. The PCR conditions were 1 cycle at

50°C for 2 minutes and at 95°C for 10 minutes followed by 40 cycles at 95°C for 15 s and at 60°C for 1 minute.

Western Blot Analysis. Livers were homogenized in a buffer containing 20 mM trishydroxymethylaminomethane-HCl (pH 7.5), 5 mM ethylene diamine tetraacetic acid, 1% NP-40, and a protease inhibitor cocktail (Pierce, Rockford, IL). Homogenated proteins (30 μg/lane) were separated by 4%-20% gradient sodium dodecyl sulfate–polyacrylamide gels (Daiichi Chemicals, Tokyo, Japan) and resolved with 130 V over 2 hours. Proteins were transferred to polyvinylidene difluoride membranes (Millipore, Billerica, MA) with a Transblot apparatus (Bio-Rad, Hercules, CA). The membranes were blocked in a buffer containing 5% nonfat milk, 50 mM trishydroxymethylaminomethane (pH 7.6), 150 mM NaCl, and 0.1% Tween 20 [trishydroxymethylaminomethane-buffered saline Tween 20 (TBS-T)] for 12 hours at 4°C. They were then probed with the monoclonal anti–4-hydroxy-2-nonenal (4-HNE) antibody (NOF, Tokyo, Japan) at a 1:200 dilution, with the polyclonal anti–insulin receptor substrate 2 (IRS-2) antibody (Millipore) at a 1:500 dilution, or with the polyclonal anti–glyceraldehyde 3-phosphate dehydrogenase antibody (Santa Cruz Biotechnology, Santa Cruz, CA) at a 1:3000 dilution in 5% bovine serum albumin TBS-T for 12 hours at 4°C. After the membranes had been washed in TBS-T, the blots were incubated with the horseradish peroxidase–linked secondary antibody (Cell Signaling Technology, Beverly, MA). Signals were detected with a chemiluminescence detection system (ECL Plus, GE Healthcare Bio-Sciences, Piscataway, NJ) and exposure to X-ray film. The hepatic 4-HNE contents were quantified with WinROOF version 5.7 (Mitani Shoji).
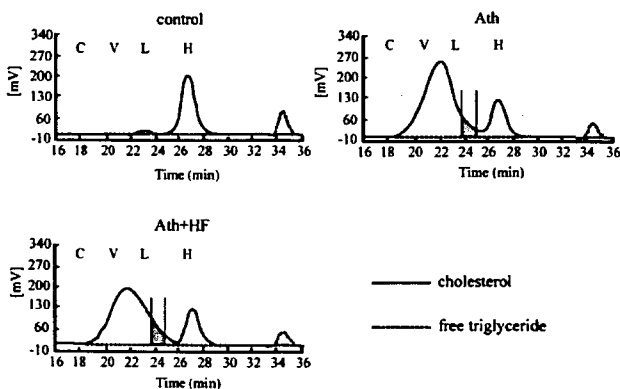

Fig. 2. HPLC analysis of plasma lipoproteins: fractionation by HPLC of cholesterol and free TG from mouse plasma after 24 weeks on the diet. The chromatograms for 1 representative sample are presented. The chylomicron, VLDL-C, LDL-C, and HDL-C fractions are labeled C, V, L, and H, respectively. The shaded fractions correspond to the level of small dense LDL-C.

Table 2. Effects of the 3 Diets on Body Weight and Lipid Levels at 6 or 24 Weeks of Feeding

Diet type	6 weeks			24 weeks		
	Control (n = 3)	Ath (n = 3)	Ath+HF (n =3)	Control (n = 4)	Ath (n = 6)	Ath+HF (n = 6)
Body weight (g)	24.7 ± 0.5	24.9 ± 0.4	23.2 ± 0.4	29.0 ± 0.7	28.1 ± 1.8	26.4 ± 1.1**
Epididymal fat pad weight (g)	0.14 ± 0.01	0.15 ± 0.01	0.15 ± 0.02	0.25 ± 0.01	0.09 ± 0.01**	0.17 ± 0.01**
Plasma triglycerides (mg/dL)	68.0 ± 5.2	54.6 ± 10.1	24.0 ± 3.6**	41.5 ± 4.6	33.8 ± 3.5	20.8 ± 1.7*
Plasma total cholesterol (mg/dL)	85.0 ± 8.5	173.6 ± 5.3**	168.1 ± 5.3**	84.6 ± 3.8	257.1 ± 10.8**	204.4 ± 8.8**
Plasma free cholesterol (mg/dL)	23.9 ± 2.2	45.9 ± 2.7**	40.2 ± 0.7**	17.3 ± 0.3	47.5 ± 5.6**	31.3 ± 2.3*
Plasma FFA (mEq/L)	0.58 ± 0.09	0.75 ± 0.10	0.46 ± 0.07	0.48 ± 0.04	0.48 ± 0.04	0.24 ± 0.06*
Plasma insulin (μU/mL)	N.D.	N.D.	N.D.	6.2 ± 0.3	11.2 ± 1.7	13.8 ± 2.9
Fasting blood glucose (mg/dL)	N.D.	N.D.	N.D.	93 ± 4	85 ± 4	93 ± 8
HOMA-IR	N.D.	N.D.	N.D.	1.4 ± 0.1	2.3 ± 0.3	3.1 ± 0.4*
Hepatic triglycerides (μg/mg protein)	67.2 ± 10.4	89.3 ± 19.7	150.8 ± 21.6*	148.6 ± 20.9	52.8 ± 17.4*	64.5 ± 9.2*
Hepatic total cholesterol (μg/mg protein)	42.0 ± 2.8	206.8 ± 22.5**	342.8 ± 40.8**	34.3 ± 2.2	143.5 ± 24.1*	192.8 ± 25.0**
Hepatic free cholesterol (μg/mg protein)	22.1 ± 3.9	30.4 ± 4.2	52.6 ± 6.6*	19.9 ± 2.3	33.0 ± 2.6*	30.9 ± 5.9
Hepatic FFA (μEq/mg protein)	45.6 ± 4.0	52.6 ± 3.3	63.0 ± 2.8*	53.1 ± 1.8	81.1 ± 6.3*	83.6 ± 8.7*

Data are means ± SEM. Significantly different from control value: $*P < 0.05$; $**P < 0.01$. Abbreviations: FFA, free fatty acid; HOMA-IR, homeostasis model assessment insulin resistance; N.D., Not determined.

Statistical Analysis. The results are shown as the means ± the standard error of the mean (SEM). The data were analyzed with a 1-way analysis of variance to compare the means of all groups. The Bonferroni multiple-comparison procedure was used to determine which pairs of means were different. Differences in the histological scores between the Ath and Ath+HF groups were compared with the Mann-Whitney U test. All calculations were performed with SPSS version 12.0 software for Windows (SPSS, Chicago, IL).
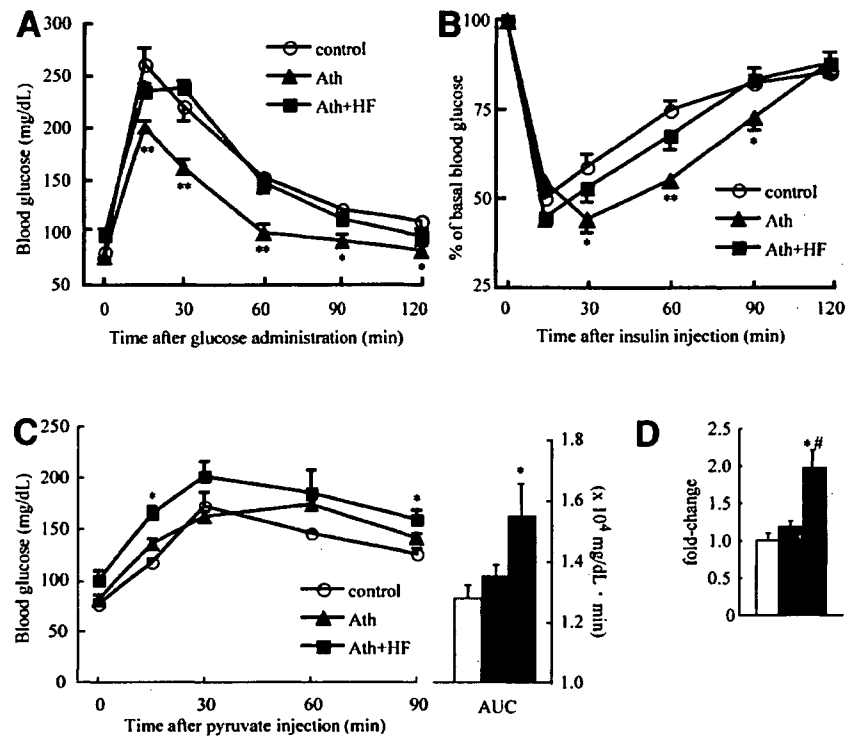
Results

Ath Diet Causes Hepatomegaly and Liver Injury. Hepatomegaly was observed in the Ath and Ath+HF groups (Fig. 1A). As shown in Fig. 1B, the livers of mice fed the Ath diet were grossly enlarged and pale in color. The serum ALT level was also elevated in the Ath and Ath+HF groups (Fig. 1C). Splenomegaly, frequently associated with cirrhosis, was detected in the Ath and Ath+HF groups at 24 weeks.

Effect of the Ath Diet on the Plasma Lipid Levels and Hepatic Lipid Content. As shown in Table 2, the plasma cholesterol levels were significantly elevated in the Ath diet group after both 6 and 24 weeks. An HPLC analysis revealed that the Ath and Ath+HF diets markedly increased the very low density lipoprotein-cholesterol (VLDL-C), low-density lipoprotein-cholesterol (LDL-C), and small dense LDL-C fractions, whereas they lowered high-density lipoprotein-cholesterol (HDL-C) in comparison with the controls (Fig. 2). As reported previously, we also confirmed atherosclerotic lesions in the mice fed the Ath and Ath+HF diets but not in the mice fed normal chow (data not shown).

The Ath and Ath+HF diets accumulated cholesterol in the liver after both 6 and 24 weeks. In addition to cholesterol, TG and FFA also accumulated with the Ath+HF diet. In comparison with hepatic lipid levels after 6 weeks, cholesterol and TG decreased in the livers of mice fed the Ath and Ath+HF diets after 24 weeks, and this indicated the progression of extensive hepatic fibrosis and impaired hepatocellular function. As is often found in patients with advanced liver disease, the serum ALT levels decreased with the progression of hepatic fibrosis, probably because of the impaired regeneration of hepatocytes and the production of ubiquitous liver enzymes.[22]

Effects of the Ath Diet on Systemic or Hepatic Insulin Resistance. GTT and ITT after 12 weeks showed that the mice fed the Ath diet were remarkably sensitive to insulin (Fig. 3A,B). This ameliorating effect on the glucose tolerance and insulin sensitivity may be attributable to decreased adipose tissue in the mice fed the Ath or Ath+HF diet (Table 2). Therefore, we next evaluated the hepatic insulin sensitivity. For this purpose, we performed the pyruvate challenge test, an established method for evaluating hepatic insulin sensitivity,[15,16] by investigating the rise in blood glucose in response to the administration of pyruvate, a precursor for gluconeogenesis. The mice fed the Ath+HF diet showed an increased rise in the blood glucose concentration after pyruvate injection (Fig. 3C) compared with the mice fed the standard chow, and this suggested that the Ath+HF diet causes hepatic insulin resistance. Furthermore, as shown in Table 2, the homeostasis model assessment of insulin resistance (HOMA-IR) was significantly higher in the mice fed the Ath+HF diet than in the control mice. The expression of messenger RNA (mRNA) for phosphoenolpyruvate carboxykinase, the rate-controlling enzyme of

Fig. 3. Evaluation of glucose tolerance and insulin sensitivity. (A) GTT and (B) ITT after 12 weeks on standard chow (n = 4), the Ath diet (n = 5), or the Ath+HF diet (n = 5). (C) Pyruvate challenge test after 6 weeks on standard chow (n = 4), the Ath diet (n = 4), or the Ath+HF diet (n = 4). The area under the curve (AUC) of the blood glucose levels during the pyruvate challenge test was calculated. (D) mRNA levels of phosphoenolpyruvate carboxykinase genes in the livers of mice fed standard chow (white bar; n = 3), the Ath diet (gray bar; n = 3), or the Ath+HF diet (black bar; n = 3) after 12 weeks. The gene expression was normalized with eukaryotic 18S ribosomal RNA. The degree of change in the gene expression was based on the mean expression levels in control mice. The values represent the means ± the SEM. *$P < 0.05$ and **$P < 0.01$ versus the control group. #$P < 0.05$ versus the Ath group.

gluconeogenesis for which the expression is negatively regulated by insulin, was significantly higher in the mice fed the Ath+HF diet than in the control mice (Fig. 3D). These results suggest that the Ath+HF diet causes hepatic insulin resistance.

Ath Diet Induces Steatosis, Fibrosis, and Cellular Ballooning of the Liver. Figure 4 shows the time course of histological changes in the livers of mice fed the Ath or Ath+HF diet. The Ath diet induced progressive steatosis, inflammation, and fibrosis in a time-dependent manner from 6-24 weeks. Moreover, cellular ballooning, an important histological feature for the diagnosis of human NASH, was observed in the Ath group after 24 weeks. The addition of a high-fat component to the Ath diet accelerated the development of steatosis, inflammation, and fibrosis. Furthermore, before the Ath group, cellular ballooning was already observed in the Ath+HF group after 12 weeks. The hepatic hydroxyproline content, an indicator of collagen accumulation in the liver, increased significantly in the mice fed the Ath diet and increased further in the mice fed the Ath+HF diet (Fig. 4C). Therefore, the Ath diet induces steatohepatitis, and the addition of a high-fat component exacerbates the histological severity of steatohepatitis and hepatic insulin resistance.

High-Fat Component Further Enhances the Activation of Hepatic Stellate Cells (HSCs) with the Ath Diet. The major sources of collagen and other extracellular matrix proteins in liver fibrosis are HSCs.[23] In re-

sponse to stimuli such as oxidative stress and inflammatory cytokines, HSCs become activated and transform into proliferative fibrogenic cells.[24] We performed an immunohistochemical analysis of α-SMA, an activated HSC marker, at different times. Representative photomicrographs of liver sections stained with the anti–α-SMA antibody are shown in Fig. 5A. We quantified the areas in the liver sections positive for α-SMA morphometrically in the 3 groups at different times as described (Fig. 5A, lower panel). The activation of HSCs was promoted in the livers of mice fed the Ath diet in a time-dependent manner from 6-24 weeks and was further accelerated by the addition of a high-fat component to the Ath diet.

To evaluate oxidative stress causing HSC activation, we assayed proteins modified with 4-HNE, which is a major aldehyde end product of membrane lipid peroxidation due to oxidative stress (Fig. 5B). In concert with the increase in α-SMA–positive cells, 4-HNE–modified proteins accumulated in the livers of mice fed the Ath diet and further accumulated in those of mice fed the Ath+HF diet. In addition to 4-HNE–modified proteins, hepatic protein carbonyls, another marker of oxidative stress, also increased with the Ath and Ath+HF diets (Fig. 5C). These results are consistent with the observation that the Ath+HF diet induced more severe inflammation and fibrosis than the Ath diet.
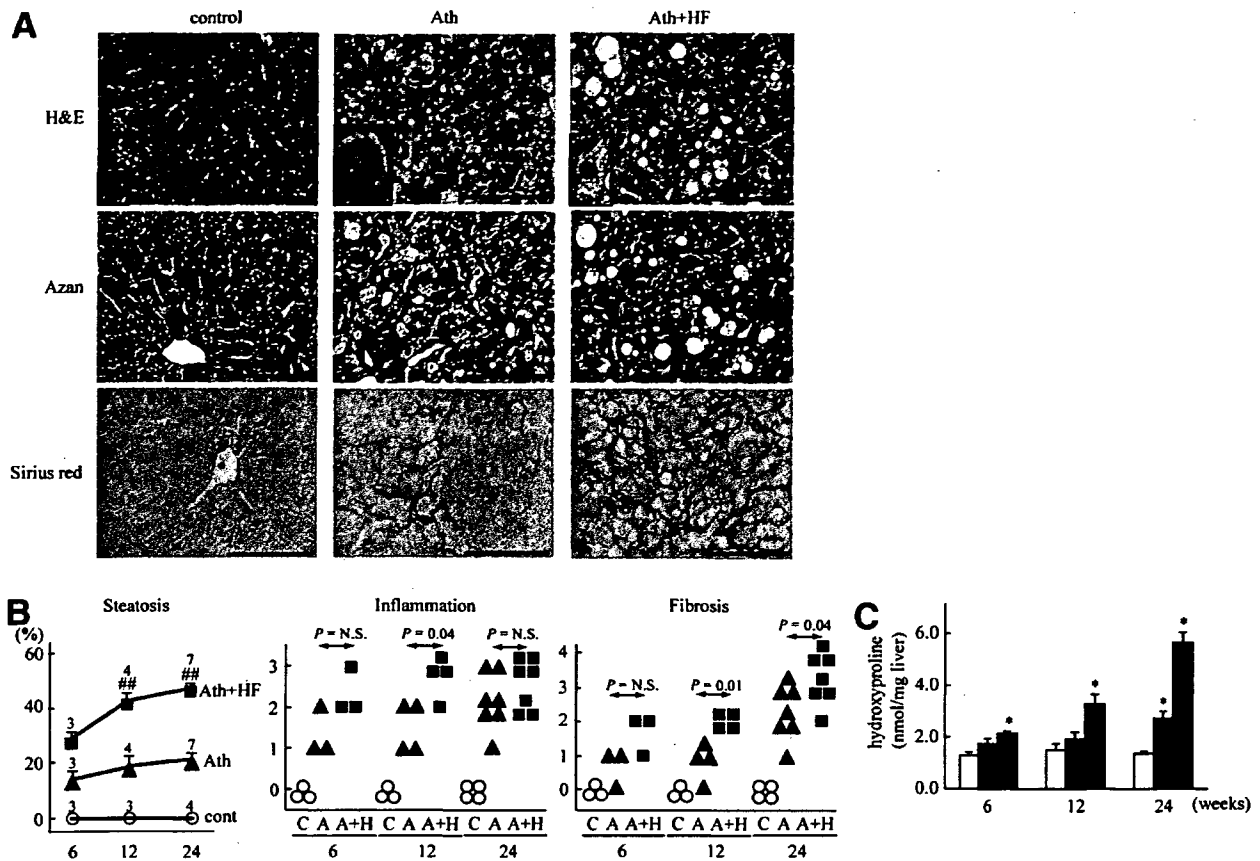
Fig. 4. Representative liver histology, scoring, and occurrence of hepatocyte ballooning. (A) Liver sections were stained with H&E, Azan, and Sirius red after 6, 12, and 24 weeks. The arrows indicate infiltration of the inflammatory cells in the hepatic parenchyma. The characteristic initial pattern of fibrosis in steatohepatitis is collagen deposition, as identified by blue and red staining. The original magnification was ×200. The scale bars represent 10 μm. Ballooning hepatocytes were seen only in the Ath and Ath+HF groups (shown in the inset). (B) The absolute percentage of the macrovesicular fat droplet area in the H&E-stained area was determined to evaluate steatosis. The values represent the means ± the SEM. The number of animals per group is indicated just above the points. ##$P < 0.01$ versus the Ath group. Inflammation and fibrosis scores were assigned in a blinded fashion to H&E-stained samples for inflammation and to Azan-stained samples for fibrosis. The criteria for each score are described in the Materials and Methods section. Differences in the inflammation and fibrosis histological scores between the Ath and Ath+HF groups were compared with the Mann-Whitney U test. The control, Ath, and Ath+HF groups are labeled C (white circles), A (gray triangles), and A+H (black squares), respectively. (C) The hydroxyproline content was determined in the livers of mice fed standard chow (white bars; n = 3), the Ath diet (gray bars; n = 3), or the Ath+HF diet (black bars; n = 3) at 6, 12, and 24 weeks. The values represent the means ± the SEM. **$P < 0.01$ versus the control group. ##$P < 0.01$ versus the Ath group.

Gene Expression in the Livers of Mice Fed the Ath Diet.

To address the molecular basis of Ath diet–induced steatohepatitis, we performed a microarray analysis, using livers at early (6 weeks) and precirrhosis stages (24 weeks) in the development of steatohepatitis. We screened 103 pathways determined with GenMAPP and extracted the metabolic pathways significantly altered in the livers of the mice fed the Ath and Ath+HF diets (Table 3). In the livers of the mice fed the Ath diet, genes involved in the inflammatory response and p38 mitogen-activated protein kinase (MAPK) signaling pathway were up-regulated significantly, whereas genes involved in fatty acid β-oxidation were down-regulated significantly in the early stage (6 weeks), and this was followed by coordinated up-reg-

ulation of the genes involved in fibrogenesis, such as the transforming growth factor β (TGF-β) signaling pathway, in the late stage (24 weeks). Adding the high-fat component to the Ath diet accelerated the up-regulation of the genes involved in inflammation (electron-transport chain, p38 MAPK signaling pathway, and Fas pathway and stress induction) and fibrogenesis (TGF-β signaling pathway and matrix metalloproteinases). Of these pathways altered in the models, we present the expression levels of representative genes involved in lipid metabolism, inflammation, oxidative stress, and fibrogenesis in Fig. 6 and Supplementary Table 2.

In the livers of mice fed the Ath diet, the expression of genes for fatty acid synthesis, such as sterol regulatory
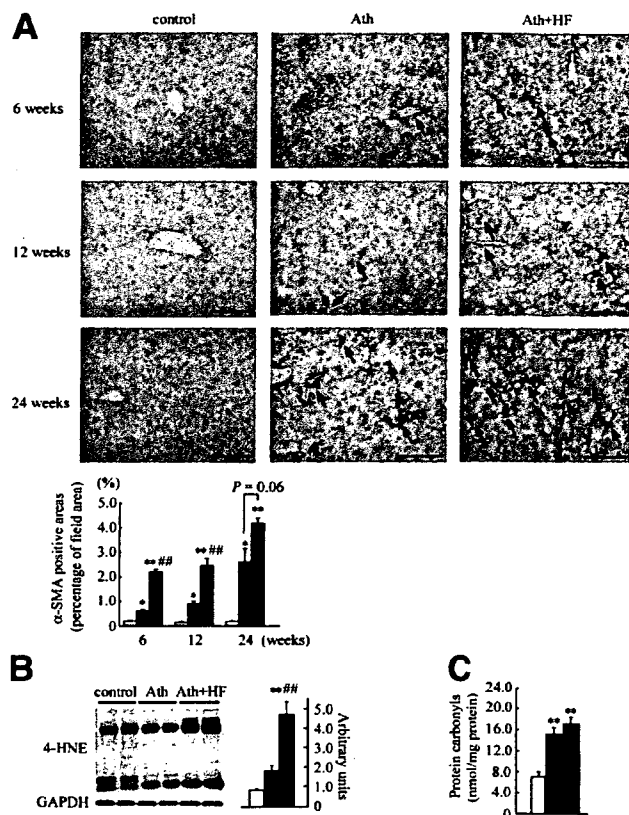
Fig. 5. Activation of HSCs and oxidative stress in the livers of mice fed the Ath or Ath+HF diet. (A) Hepatic α-SMA-positive cells (indicated by arrows) were detected by immunohistochemical staining at 6, 12, or 24 weeks. The original magnification was ×200. The scale bars represent 10 μm. The α-SMA-positive area was quantified morphometrically in the liver sections of mice fed standard chow (white bar; n = 3), the Ath diet (gray bar; n = 3), or the Ath+HF diet (black bar; n = 3) at different times, as described in the Materials and Methods section. (B) Western blot of 4-HNE-modified proteins in the liver after 24 weeks. The hepatic content of 4-HNE-modified proteins was quantified in mice fed standard chow (white bar; n = 4), the Ath diet (gray bar; n = 4), or the Ath+HF diet (black bar; n = 4), as described in the Materials and Methods section. (C) Hepatic protein carbonyls were determined in the mice fed standard chow (white bar; n = 3), the Ath diet (gray bar; n = 4), or the Ath+HF diet (black bar; n = 4) after 24 weeks, as described in the Materials and Methods section. The values represent the means ± the SEM. *P < 0.05 and **P < 0.01 versus the control group. #P < 0.05 and ##P < 0.01 versus the Ath group.

element binding protein 1c (SREBP-1c), a transcriptional regulator of fatty acid synthesis,[25] and fatty acid synthase (FAS), was coordinately up-regulated. In contrast, the expression levels of genes for the mitochondrial fatty acid β-oxidation pathway were coordinately repressed in concert with a decrease in the expression of peroxisome proliferator-activated receptor α (PPARα), a transcriptional up-regulator of fatty acid β-oxidation in the liver.[26] It is recognized that mitochondrial β-oxidation and the levels of carnitine palmitoyltransferase 1a (CPT-1a) and PPARα expression are increased compensatively in the

livers of patients with NAFLD[27,28] and obese-diabetic (ob/ob) mice with severe steatosis of the liver.[29] Therefore, although the levels of PPARα and CPT-1a mRNA expression in the Ath+HF group were higher than those in the Ath group, it may not have been enough to metabolize the excessive fatty acids from the high-fat component and intrahepatic fatty acid synthesis.

It is believed that oxidative stress due to the generation of reactive oxygen species (ROS) or decreased antioxidant defenses is directly involved in the development of steatohepatitis.[30] The expression levels of genes for the reduced-form nicotinamide adenine dinucleotide phosphate (NADPH) oxidase complex, an important source of ROS,[31] were coordinately elevated in mice fed the Ath diet and further up-regulated in mice fed the Ath+HF diet.

The Ath diet has previously been reported to induce the expression of genes for inflammation.[32,33] Our results further demonstrate that inflammatory cytokines, such as tumor necrosis factor α (TNF-α), chemokines, and their receptors, are up-regulated in mice fed the Ath diet.

The Ath diet also induced genes involved in collagen accumulation, especially after 24 weeks. At 6 weeks, the expression levels of collagen genes were higher in the Ath+HF group than in the Ath group (Fig. 6). In addition, the expression levels of genes for TGF-β and plasminogen activator inhibitor 1 (PAI-1), key inducers of fibrogenesis, were dramatically up-regulated in the Ath+HF group compared with the Ath group at 24 weeks. These results support the finding that the Ath+HF diet induces more rapid progression of steatohepatitis than the Ath diet.

Discussion

Whether cholesterol, TG, or FFA contributes to the development of NASH remains controversial.[34] Because the feeding of cholesterol and cholic acid, which are the main components of the Ath diet, leads to the additive accumulation of cholesterol in the liver, the main pathology in Ath diet–induced steatohepatitis is caused by cholesterol-induced toxicity.[35]

In this study, we have shown that Ath diet–induced steatohepatitis with atherosclerosis is a better experimental model of human NASH for the following reasons: (1) this model seems to be a more physiological dietary model of NASH than existing animal models, which require genetic defects, chemical agents such as carbon tetrachloride, or the depletion of nutrients, such as the MCD diet–induced model; (2) the liver pathology involves steatohepatitis with cellular ballooning, a necessary histological feature defining human NASH; (3) the addition of a high-fat component to the Ath diet causes hepatic insulin

Table 3. Biological Pathways of Liver Genes Regulated by the Ath or Ath+HF Diets After 6 or 24 Weeks

| Pathway Name	Number of Genes Changed	Number of Genes Measured	Z Score	Permuted P Value
Ath diet				
Up-regulated at 6 weeks				
Inflammatory Response	23	41	3.22	< 0.01
DNA replication Reactome	21	41	2.56	0.010
Cell Cycle-G1 to S control Reactome	32	68	2.56	0.016
G1 to S cell cycle Reactome	32	68	2.56	0.016
RNA transcription Reactome	20	40	2.36	0.036
p38 MAPK signaling	15	28	2.38	0.037
Down-regulated at 6 weeks				
Amino Acid Metabolism	23	45	2.94	< 0.01
Cholesterol Biosynthesis	11	15	3.56	< 0.01
Complement and Coagulation Cascades	29	59	3.04	< 0.01
Mitochondrial fatty acid betaoxidation	11	16	3.28	< 0.01
Blood Clotting Cascade	11	18	2.77	0.012
Unsaturated Fatty Acid Beta Oxidation	5	6	2.78	0.014
Biogenic Amine Synthesis	8	14	2.13	0.042
Krebs-TCA Cycle	14	29	2.03	0.045
Up-regulated at 24 weeks				
mRNA processing binding Reactome	196	438	5.91	< 0.01
TGF Beta Signaling Pathway	62	124	4.37	< 0.01
Translation Factors	27	49	3.50	< 0.01
Complement Activation Classical	9	15	2.34	0.021
Down-regulated at 24 weeks				
GPCRDB Other	52	147	3.58	< 0.01
Small ligand GPCRs	11	19	3.61	< 0.01
Synthesis and Degradation of Ketone Bodies	4	4	3.66	< 0.01
Mitochondrial fatty acid betaoxidation	9	16	3.16	< 0.01
Cholesterol Biosynthesis	8	15	2.79	< 0.01
Metabotropic glutamate pheromone	6	10	2.78	0.020
Ath + HF diet				
Up-regulated at 6 weeks				
Electron Transport Chain	35	82	4.93	< 0.01
mRNA processing binding Reactome	120	434	3.64	< 0.01
Translation Factors	20	49	3.48	< 0.01
p38 MAPK signaling pathway	13	28	3.36	< 0.01
Unsaturated Fatty Acid Beta Oxidation	4	6	2.78	0.018
Matrix Metalloproteinases	9	24	2.03	0.034
TGF Beta Signaling Pathway	35	124	2.08	0.039
Fas pathway and stress induction	41	149	2.07	0.042
Down-regulated at 6 weeks				
Focal adhesion	56	186	3.51	< 0.01
Steroid Biosynthesis	8	12	4.06	< 0.01
Complement and Coagulation Cascades	20	59	2.70	< 0.01
G Protein Signaling	26	83	2.62	0.013
Calcium regulation in cardiac cells	41	145	2.54	0.014
Cholesterol Biosynthesis	7	15	2.60	0.016
Up-regulated at 24 weeks				
Translation Factors	21	49	3.993	< 0.01
mRNA processing binding Reactome	121	437	4.055	< 0.01
p38 MAPK signaling pathway	12	28	3.016	< 0.01
TGF Beta signaling pathway	35	124	2.077	0.039
Down-regulated at 24 weeks				
Amino Acid Metabolism	19	45	3.891	< 0.01
Urea cycle and metabolism of amino groups	10	20	3.472	< 0.01
Striated muscle contraction	16	42	3.080	< 0.01
Steroid Biosynthesis	6	12	2.689	0.015
Small ligand GPCRs	8	19	2.513	0.020
Glycolysis and Gluconeogenesis	14	41	2.402	0.023
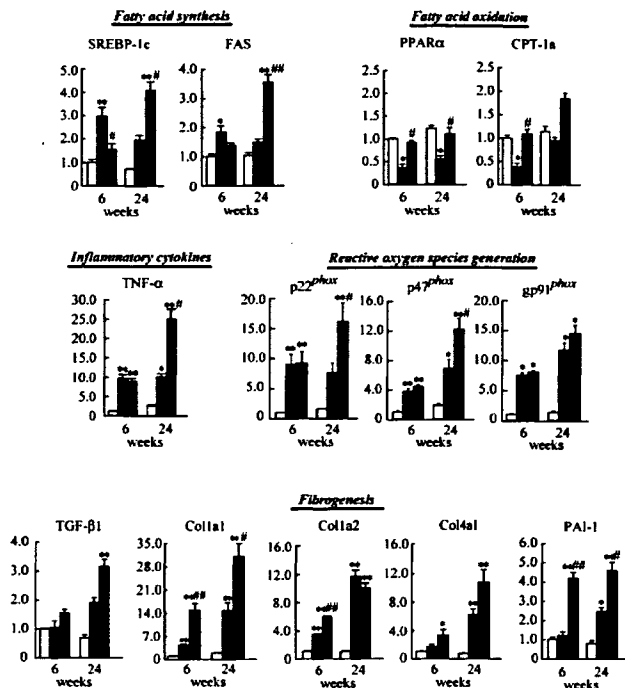
Fig. 6. Quantitative real-time PCR for representative genes involved in steatohepatitis. The mRNA levels of genes for SREBP-1c, FAS, PPARα, CPT-1a, TNF-α, p22phox, p47phox, gp91phox, TGF-β1, procollagen type I alpha 1 (Col1a1), procollagen type I alpha 2 (Col1a2), procollagen type IV alpha 1 (Col4a1), and PAI-1 in the livers of mice fed standard chow (n = 3), the Ath diet (n = 3), or the Ath+HF diet (n = 3) were quantified with real-time PCR after 6 and 24 weeks. The RNA samples used for real-time PCR were the same as those used for the microarray analysis. The gene expression was normalized with eukaryotic 18S ribosomal RNA. The degree of change in the gene expression was based on the mean expression levels of control mice at 6 weeks. The values represent the means ± SEM. *$P < 0.05$ and **$P < 0.01$ versus the control group. #$P < 0.05$ and ##$P < 0.01$ versus the Ath group.

resistance and promotes oxidative stress, the activation of HSCs, and all components of the liver pathology of NASH (steatosis, inflammation, fibrosis, and cellular ballooning); and (4) there is a molecular signature indicative of lipid-induced oxidative stress in the liver, which may play a causal role in the development of steatohepatitis.

To diagnose human NASH, cellular ballooning, in addition to simple steatosis and inflammatory cell infiltration, is one of the most important pathological features.[36] However, ballooning degeneration has scarcely been determined in the existing animal models, including mice fed the MCD diet. We believe that our study is the first to report that cellular ballooning is frequently induced in the livers of mice fed the Ath diet.

Recently, we proved that insulin resistance accelerates the pathological development of steatohepatitis experimentally.[11] In this study, on the basis of the results of the pyruvate challenge test and HOMA-IR, we concluded that the Ath+HF diet causes hepatic insulin resistance. It

is known that the excessive accumulation of FFAs caused by the overexpression of lipoprotein lipase[37] and an increase in SREBP-1c–regulated lipogenesis[38] leads to impaired tyrosine phosphorylation of IRS-1 and IRS-2, resulting in hepatic insulin resistance. Furthermore, the up-regulation of SREBP-1c–regulated lipogenesis contributes to the development of insulin resistance via the down-regulation of IRS-2 in the liver.[39,40] Indeed, in our study, the induction of lipoprotein lipase and SREBP-1c and the repression of IRS-2 were detected in the livers of mice fed the Ath diet (Fig. 7). Moreover, the up-regulation of stearoyl–coenzyme A desaturase 1, an enzyme that catalyzes the synthesis of monounsaturated fatty acids, might contribute to lipid accumulation and insulin resistance in the liver, as reported in skeletal muscle.[41] Therefore, the cholesterol-induced and TG-induced alteration of fatty acid metabolism may cause hepatic insulin resistance in this model of steatohepatitis.

Another possible cause of the liver pathology in our model is lipid-induced oxidative stress and its downstream events, as we identified an accumulation of 4-HNE and protein carbonyls, the activation of stellate cells, and hepatic inflammation with cell ballooning. In this study, in addition to cholesterol, the accumulation of TG and FFAs by the addition of a high-fat component accelerated oxidative stress, possibly via the up-regulation of genes involved in the generation of ROS, such as the NADPH oxidase complex, and the down-regulation of genes for antioxidant enzymes. While we were preparing this article, Mari et al.[35] reported that the mitochondrial loading of free cholesterol, but not TG and FFA, decreases mitochondrial glutathione and sensitizes it to the TNF-α–mediated apoptosis of hepatocytes. Therefore, the different kinds of accumulated lipids may cause oxidative stress in the liver additively in different ways. In
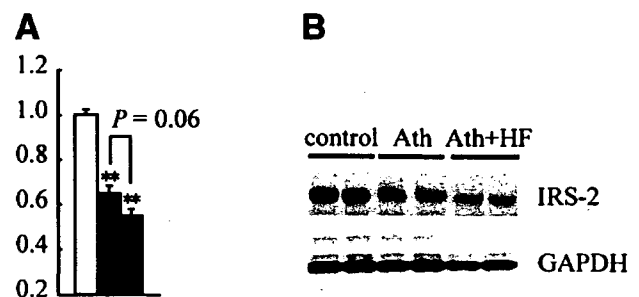
Fig. 7. The Ath and Ath+HF diets decreased the mRNA and protein levels of IRS-2 in the liver. (A) mRNA levels of the IRS-2 genes in the livers of mice fed standard chow (white bar; n = 3), the Ath diet (gray bar; n = 3), or the Ath+HF diet (black bar; n = 3) after 12 weeks. The values represent the means ± the SEM. *$P < 0.05$ versus the control group. #$P < 0.05$ versus the Ath group. (B) Western blot of IRS-2 in the livers of mice fed the standard chow, Ath diet, or Ath+HF diet after 12 weeks.

patients with NASH, impaired glutathione metabolism and antioxidant enzyme activity probably cause an increase in oxidative stress.[42]

The Ath diet induces an Ath lipid profile, including an increase in small dense LDL-C, which is highly susceptible to oxidation, and then leads to oxidized low-density lipoprotein (LDL), which induces an inflammatory response in endothelial cells.[43] In the livers of mice fed the Ath diet, the expression levels of genes for CD36 antigen and scavenger receptor type B member 1, which are receptors for oxidized LDL,[44] tended to be up-regulated (Supplementary Table 2). Therefore, it might be possible that up-regulated receptors for oxidized LDL enhance the uptake of increasing levels of small dense LDL-C and contribute to inflammation in the liver.

In response to the lipid-induced oxidative stress, genes involved in fibrogenesis were coordinately up-regulated. Indeed, the hepatic expression of TNF-α and NADPH oxidase complex genes preceded that of fibrogenic genes, and this suggested that inflammation precedes the fibrogenic process in our models. The expression of TGF-β and PAI-1 genes was up-regulated dramatically, especially in the Ath+HF group. PAI-1 is a key factor in matrix remodeling, and the gene is highly induced in response to TGF-β.[45] Urokinase plasminogen activator generates plasmin, and this process is inhibited by PAI-1. Plasmin degrades the extracellular matrix both directly and by activating matrix metalloproteinases.[46] Therefore, PAI-1 inhibits collagenolysis by inhibiting the generation of plasmin in the liver. Consequently, the inhibition of collagenolysis, in addition to the overall up-regulation of collagen genes, might contribute to hepatic fibrosis in this model.

In summary, we report that the Ath diet induces steatohepatitis with cellular ballooning via cholesterol-induced oxidative stress and hepatic insulin resistance. Adding a high-fat component further aggravates oxidative stress and steatohepatitis, possibly by inducing insulin resistance and down-regulating genes for antioxidant enzymes. This model suggests the critical and different roles of cholesterol, TG, and FFAs in causing oxidative stress and insulin resistance leading to steatohepatitis and provides a system for screening therapeutic targets to treat NASH and atherosclerosis.

References

1. Marchesini G, Bugianesi E, Forlani G, Cerrelli F, Lenzi M, Manini R, et al. Nonalcoholic fatty liver, steatohepatitis, and the metabolic syndrome. HEPATOLOGY 2003;37:917-923.

2. Sanyal AJ. AGA technical review on nonalcoholic fatty liver disease. Gastroenterology 2002;123:1705-1725.

3. James OF, Day CP. Non-alcoholic steatohepatitis (NASH): a disease of emerging identity and importance. J Hepatol 1998;29:495-501.

4. Targher G, Bertolini L, Poli F, Rodella S, Scala L, Tessari R, et al. Nonalcoholic fatty liver disease and risk of future cardiovascular events among type 2 diabetic patients. Diabetes 2005;54:3541-3546.

5. Chen H, Charlat O, Tartaglia LA, Woolf EA, Weng X, Ellis SJ, et al. Evidence that the diabetes gene encodes the leptin receptor: identification of a mutation in the leptin receptor gene in db/db mice. Cell 1996;84:491-495.

6. Shimano H, Horton JD, Hammer RE, Shimomura I, Brown MS, Goldstein JL. Overproduction of cholesterol and fatty acids causes massive liver enlargement in transgenic mice expressing truncated SREBP-1a. J Clin Invest 1996;98:1575-1584.

7. Surwit RS, Feinglos MN, Rodin J, Sutherland A, Petro AE, Opara EC, et al. Differential effects of fat and sucrose on the development of obesity and diabetes in C57BL/6J and A/J mice. Metabolism 1995;44:645-651.

8. Weltman MD, Farrell GC, Liddle C. Increased hepatocyte CYP2E1 expression in a rat nutritional model of hepatic steatosis with inflammation. Gastroenterology 1996;111:1645-1653.

9. Leclercq IA, Farrell GC, Field J, Bell DR, Gonzalez FJ, Robertson GR. CYP2E1 and CYP4A as microsomal catalysts of lipid peroxides in murine nonalcoholic steatohepatitis. J Clin Invest 2000;105:1067-1075.

10. Rinella ME, Green RM. The methionine-choline deficient dietary model of steatohepatitis does not exhibit insulin resistance. J Hepatol 2004;40:47-51.

11. Ota T, Takamura T, Kurita S, Matsuzawa N, Kita Y, Uno M, et al. Insulin resistance accelerates a dietary rat model of nonalcoholic steatohepatitis. Gastroenterology 2007;132:282-293.

12. Paigen B, Morrow A, Brandon C, Mitchell D, Holmes P. Variation in susceptibility to atherosclerosis among inbred strains of mice. Atherosclerosis 1985;57:65-73.

13. Jeong WI, Jeong DH, Do SH, Kim YK, Park HY, Kwon OD, et al. Mild hepatic fibrosis in cholesterol and sodium cholate diet-fed rats. J Vet Med Sci 2005;67:235-242.

14. Usui S, Hara Y, Hosaki S, Okazaki M. A new on-line dual enzymatic method for simultaneous quantification of cholesterol and triglycerides in lipoproteins by HPLC. J Lipid Res 2002;43:805-814.

15. Miyake K, Ogawa W, Matsumoto M, Nakamura T, Sakaue H, Kasuga M. Hyperinsulinemia, glucose intolerance, and dyslipidemia induced by acute inhibition of phosphoinositide 3-kinase signaling in the liver. J Clin Invest 2002;110:1483-1491.

16. Yamauchi T, Nio Y, Maki T, Kobayashi M, Takazawa T, Iwabu M, et al. Targeted disruption of AdipoR1 and AdipoR2 causes abrogation of adiponectin binding and metabolic actions. Nat Med 2007;13:332-339.

17. Brunt EM, Janney CG, Di Bisceglie AM, Neuschwander-Tetri BA, Bacon BR. Nonalcoholic steatohepatitis: a proposal for grading and staging the histological lesions. Am J Gastroenterol 1999;94:2467-2474.

18. Folch J, Lees M, Sloane Stanley GH. A simple method for the isolation and purification of total lipides from animal tissues. J Biol Chem 1957;226:497-509.

19. Bataller R, Schwabe RF, Choi YH, Yang L, Paik YH, Lindquist J, et al. NADPH oxidase signal transduces angiotensin II in hepatic stellate cells and is critical in hepatic fibrosis. J Clin Invest 2003;112:1383-1394.

20. Doniger SW, Salomonis N, Dahlquist KD, Vranizan K, Lawlor SC, Conklin BR. MAPPFinder: using Gene Ontology and GenMAPP to create a global gene-expression profile from microarray data. Genome Biol 2003;4:R7.

21. Dahlquist KD, Salomonis N, Vranizan K, Lawlor SC, Conklin BR. GenMAPP, a new tool for viewing and analyzing microarray data on biological pathways. Nat Genet 2002;31:19-20.

22. Matloff DS, Selinger MJ, Kaplan MM. Hepatic transaminase activity in alcoholic liver disease. Gastroenterology 1980;78:1389-1392.

23. Friedman SL. Molecular regulation of hepatic fibrosis, an integrated cellular response to tissue injury. J Biol Chem 2000;275:2247-2250.

24. Leonarduzzi G, Scavazza A, Biasi F, Chiarpotto E, Camandola S, Vogel S, et al. The lipid peroxidation end product 4-hydroxy-2,3-nonenal up-regulates transforming growth factor beta1 expression in the macrophage lineage: a link between oxidative injury and fibrosclerosis. FASEB J 1997; 11:851-857.

25. Shimano H, Yahagi N, Amemiya-Kudo M, Hasty AH, Osuga J, Tamura Y, et al. Sterol regulatory element-binding protein-1 as a key transcription factor for nutritional induction of lipogenic enzyme genes. J Biol Chem 1999;274:35832-35839.

26. Aoyama T, Peters JM, Iritani N, Nakajima T, Furihata K, Hashimoto T, et al. Altered constitutive expression of fatty acid-metabolizing enzymes in mice lacking the peroxisome proliferator-activated receptor alpha (PPARalpha). J Biol Chem 1998;273:5678-5684.

27. Sanyal AJ, Campbell-Sargent C, Mirshahi F, Rizzo WB, Contos MJ, Sterling RK, et al. Nonalcoholic steatohepatitis: association of insulin resistance and mitochondrial abnormalities. Gastroenterology 2001;120: 1183-1192.

28. Chalasani N, Gorski JC, Asghar MS, Asghar A, Foresman B, Hall SD, et al. Hepatic cytochrome P450 2E1 activity in nondiabetic patients with nonalcoholic steatohepatitis. HEPATOLOGY 2003;37:544-550.

29. Li Z, Yang S, Lin H, Huang J, Watkins PA, Moser AB, et al. Probiotics and antibodies to TNF inhibit inflammatory activity and improve nonalcoholic fatty liver disease. HEPATOLOGY 2003;37:343-350.

30. Day CP, James OF. Steatohepatitis: a tale of two "hits"? Gastroenterology 1998;114:842-845.

31. De Minicis S, Bataller R, Brenner DA. NADPH oxidase in the liver: defensive, offensive, or fibrogenic? Gastroenterology 2006;131:272-275.

32. Vergnes L, Phan J, Strauss M, Tafuri S, Reue K. Cholesterol and cholate components of an atherogenic diet induce distinct stages of hepatic inflammatory gene expression. J Biol Chem 2003;278:42774-42784.

33. Liao F, Andalibi A, de Beer FC, Fogelman AM, Lusis AJ. Genetic control of inflammatory gene induction and NF-kappa B-like transcription factor activation in response to an atherogenic diet in mice. J Clin Invest 1993; 91:2572-2579.

34. Ginsberg HN. Is the slippery slope from steatosis to steatohepatitis paved with triglyceride or cholesterol? Cell Metab 2006;4:179-181.

35. Mari M, Caballero F, Colell A, Morales A, Caballeria J, Fernandez A, et al. Mitochondrial free cholesterol loading sensitizes to TNF- and Fas-mediated steatohepatitis. Cell Metab 2006;4:185-198.

36. Kleiner DE, Brunt EM, Van Natta M, Behling C, Contos MJ, Cummings OW, et al. Design and validation of a histological scoring system for nonalcoholic fatty liver disease. HEPATOLOGY 2005;41:1313-1321.

37. Kim JK, Fillmore JJ, Chen Y, Yu C, Moore IK, Pypaert M, et al. Tissue-specific overexpression of lipoprotein lipase causes tissue-specific insulin resistance. Proc Natl Acad Sci U S A 2001;98:7522-7527.

38. Horton JD, Shimomura I, Brown MS, Hammer RE, Goldstein JL, Shimano H. Activation of cholesterol synthesis in preference to fatty acid synthesis in liver and adipose tissue of transgenic mice overproducing sterol regulatory element-binding protein-2. J Clin Invest 1998;101:2331-2339.

39. Ide T, Shimano H, Yahagi N, Matsuzaka T, Nakakuki M, Yamamoto T, et al. SREBPs suppress IRS-2-mediated insulin signalling in the liver. Nat Cell Biol 2004;6:351-357.

40. Nakagawa Y, Shimano H, Yoshikawa T, Ide T, Tamura M, Furusawa M, et al. TFE3 transcriptionally activates hepatic IRS-2, participates in insulin signaling and ameliorates diabetes. Nat Med 2006;12:107-113.

41. Miyazaki M, Dobrzyn A, Sampath H, Lee SH, Man WC, Chu K, et al. Reduced adiposity and liver steatosis by stearoyl-CoA desaturase deficiency are independent of peroxisome proliferator-activated receptor-alpha. J Biol Chem 2004;279:35017-35024.

42. Nobili V, Pastore A, Gaeta LM, Tozzi G, Comparcola D, Sartorelli MR, et al. Glutathione metabolism and antioxidant enzymes in patients affected by nonalcoholic steatohepatitis. Clin Chim Acta 2005;355:105-111.

43. Galeano NF, Al-Haideri M, Keyserman F, Rumsey SC, Deckelbaum RJ. Small dense low density lipoprotein has increased affinity for LDL receptor-independent cell surface binding sites: a potential mechanism for increased atherogenicity. J Lipid Res 1998;39:1263-1273.

44. Endemann G, Stanton LW, Madden KS, Bryant CM, White RT, Protter AA. CD36 is a receptor for oxidized low density lipoprotein. J Biol Chem 1993;268:11811-11816.

45. Chapman HA. Disorders of lung matrix remodeling. J Clin Invest 2004; 113:148-157.

46. Leyland H, Gentry J, Arthur MJ, Benyon RC. The plasminogen-activating system in hepatic stellate cells. HEPATOLOGY 1996;24:1172-1178.

Hepatitis B virus X protein overcomes oncogenic RAS-induced senescence in human immortalized cells

Naoki Oishi,[1,2] Khurts Shilagardi,[1] Yasunari Nakamoto,[2] Masao Honda,[2] Shuichi Kaneko[2] and Seishi Murakami[1,3]

[1]Department of Signal Transduction, Cancer Research Institute; [2]Department of Disease Control and Homeostasis, Graduate School of Medicine, Kanazawa University, 13-1 Takara-machi, Kanazawa 920-0934, Japan

Chronic infection with hepatitis B virus (HBV) is a major risk factor for hepatocellular carcinoma. The HBV X protein (HBx) is thought to have oncogenic potential, although the molecular mechanism remains obscure. Pathological roles of HBx in the carcinogenic process have been examined using rodent systems and no report is available on the oncogenic roles of HBx in human cells *in vitro*. We therefore examined the effect of HBx on immortalization and transformation in human primary cells. We found that HBx could overcome active RAS-induced senescence in human immortalized cells and that these cells could form colonies in soft agar and tumors in nude mice. HBx alone, however, could contribute to neither immortalization nor transformation of these cells. In a population doubling analysis, an N-terminal truncated mutant of HBx, HBx-D1 (amino acids 51–154), which harbors the coactivation domain, could overcome active RAS-induced cellular senescence, but these cells failed to exhibit colonigenic and tumorigenic abilities, probably due to the low expression level of the protein. By scanning a HBx expression library of the clustered-alanine substitution mutants, the N-terminal domain was found to be critical for overcoming active RAS-induced senescence by stabilizing full-length HBx. These results strongly suggest that HBx can contribute to carcinogenesis by overcoming active oncogene-induced senescence. (*Cancer Sci* 2007; 98: 1540–1548)

C hronic infection with HBV is a major risk factor for HCC worldwide. HBV belongs to the Hepadnavirus family. Its genome is a 3.2-kb, circular, partially double-stranded DNA molecule with four overlapping open reading frames: PC-C, PS-S, P and X.[1] The HBV genome, which is converted to covalently closed circular DNA in the nucleus after infection, serves as the template for transcription, generating the four viral transcripts that encode the HBV core and polymerase polypeptides, the large surface antigen polypeptide, the middle and major surface antigen polypeptides, and the HBx polypeptide. HBV replicates by reverse transcription of viral pregenomic 3.5-kb RNA using the HBV polymerase that catalyzes RNA-dependent DNA synthesis and DNA-dependent DNA synthesis.[1,2] It is converted into the 3.2-kb partially double-stranded genomic DNA inside the viral capsid.

The critical role of HBV chronic infection in HCC has been well established etiologically, whereas the mechanism by which HBV causes transformation of hepatocytes remains unclear.[3–5] HBx has long been suspected of playing a positive role in hepatocarcinogenesis, as avian hepadnaviruses missing the X open reading frame seem not to be associated with HCC. HBx consists of 154 aa and is a multifunctional regulator that modulates many host cell functions through its interactions with a variety of host factors.[5] HBx consists of both a negative regulatory domain[6] and a coactivation domain that is required for the augmentation of virus and host genes.[7,8] HBx was reported to transform rodent immortal cells *in vitro*,[9,10] and a high incidence of HCC has been reported in transgenic mice overexpressing HBx.[11,12] However, the functional role of HBx

in the transformation is still controversial. Some independent groups proposed collaborating roles of HBx in the hepatocarcinogenic process.[13–15] Although these reports are informative, all were experimentally assessed in rodent systems. Because mouse and human primary cells have different telomere biology,[16] DNA damage check point control mechanisms and cell cycle progression,[17,18] developing a human system to address the functional role of HBx is critically important. Here we report that we established human fibroblast cells stably expressing HBx protein and analyzed the effects of HBx expression on the ability to confer an immortal phenotype and tumorigenic potential.

Materials and Methods

Retroviral vectors. All constructs for the expression of HBx (subtype adr) proteins, pNKF-HBx (aa 1–154), pNKF-HBx-D1 (aa 1–50) and pNKF-HBx-D5 (aa 51–154) have been described previously.[8] The retrovirus vectors pBabe-puro, hygro, puro-H-RAS^{V12} hygro-hTERT and pWZL-blast were kindly provided by W. C. Hahn (Dana-Farber Cancer Institute, Harvard).[19,20] To construct pBabe-blast, the blasticidin S cDNA of pWZL-blast was used as a template to amplify the PCR products of blasticidin S with the primer set of AAGCTTACCATGGCCAAGCCTTTGT and ATCGATTTAGCCCTCCCACACATAA, generating an artificial *Hind*III site at the 5-end and a *Cla*I site at the 3′-end, respectively. The HBx cDNA of pNKF-HBx was used as a template to amplify the PCR products of HBx with a primer set of TGATCAATGGACTACAAAGACGAT and CTCGAGAGAT-CTTTAATTAATTAA, generating an artificial *Fba*I site at the 5-end and an *Xho*I site at the 3′-end, respectively. The PCR products were digested and inserted into the *Bam*HI and *Sal*I sites of the pBabe-blast vector. The *Eco*RI and *Bgl*II fragments of HBx-D1 and HBx-D5 from pNKF-HBx-D1 and pNKF-HBx-D5 were, respectively, inserted into the *Eco*RI and *Bgl*II sites of the pBabe-blast-HBx vectors. An alanine scanning method was applied to construct a series of HBx clustered alanine substitution mutants (designated 'cm') by site-directed mutagenesis. The mutagenesis was carried out using a splicing PCR method with all of the mutated oligonucleotide primer sets. The target sequence of seven aa residues was changed to AAASAAA, and all of the HBx-encoding DNA fragments bearing the clustered mutations were introduced into the *Eco*RI and *Bam*HI sites of pNKFLAG, generating the pNKF-Xcm1 to pNKF-Xcm21 constructs. The

*Eco*RI and *Bgl*II fragments of HBx-cm1 to HBx-cm21 from pNKF-Xcm1 to pNKF-Xcm21 were, respectively, inserted into the *Eco*RI and *Bgl*II sites of the pBabe-blast-HBx vectors. All of the constructs were sequenced by the dideoxy method using the *Taq* sequencing primer kit and a DNA sequencer (370A; Applied Biosystems).

Virus production and cell lines. Amphotropic retroviruses were produced by transfection of the 293T producer cell line with a retroviral vector and a vector encoding replication-defective helper viruses, pCL-Ampho (Imgenex), using FuGENE 6 transfection reagent (Roche Applied Science) according to the manufacturer's recommendations. Two days after the transfection, culture supernatants were collected, filtered, supplemented with 4 μg/mL polybrene, and used for infection. Two days after the infection, drug selection of infected cells was started, and the selected populations were used in all of the experiments. Infected cell populations were selected in puromycin (1.0 μg/mL), blasticidin S (4 μg/mL) and hygromycin (80 μg/mL) for up to 2 weeks.

Cell culture. Human lung fibroblasts (TIG3) from the Japanese Collection of Research Bioresources were maintained in DMEM with 10% heat-inactivated fetal bovine serum (JRH Biosciences). Human foreskin fibroblasts, BJ and BJ-hTERT-LT-ST-H-RAS^{V12} cells were maintained as described previously.[19] These human fibroblasts were not clonal and were maintained as populations. BJ cells and TIG3 cells have a finite lifespan, and were used at PD between 25 and 35. PD were determined using the formula:

$$PD = Log(Nf/Ni)/Log2,$$

where Nf = the number of cells counted and Ni = the number of cells seeded. Comparisons of means and standard deviations were carried out using the unpaired *t*-test.

Western blot analysis. Cells were harvested, washed with phosphate-buffered saline (−), and sonicated in a lysis buffer (50 mM Tris-HCl [pH 7.4], 200 mM NaCl, 1 mM ethylenediaminetetraacetic acid, 10% glycerol, 1 mM phenylmethylsulfonyl fluoride, 10 μg/mL leupeptin, 10 μg/mL aprotinin and 10 μg/mL dithiothreitol). Total lysates were fractionated by SDS-PAGE, transferred onto nitrocellulose membranes and subjected to western blot analysis with antibodies. Anti-FLAG M2 antibody and anti-β-actin antibody were from Sigma. Anti-RAS antibody F-235 (sc-29), anti-p53 antibody DO-1 (sc-126) and anti-p21 antibody F-5 (sc-6246) were from Santa Cruz. Anti-p16 antibody was from BD PharMingen. The proteins were visualized by enhanced chemiluminescence according to the manufacturer's instructions (Amersham).

Analysis of senescence. SA-β-Gal staining was carried out using the Senescence Detection Kit (Oncogene) as instructed by the manufacturer. For each sample, at least 200 cells were counted in randomly chosen fields.

Telomerase activity assays. Total lysates of cells were subjected to the telomerase repeat amplification protocol using a TRAPEZE kit (Intergen) according to the manufacturer's instructions.

Soft-agar colony formation assays. Soft-agar growth assays were carried out as described previously.[19] At the time of plating in soft agar, cultures were trypsinized and counted, and 5×10^3 or 5×10^4 total cells were mixed with 1.5 mL of 0.35% Noble agar-DMEM (top layer) and then poured on top of 5 mL of solidified 0.7% Noble agar-DMEM (bottom layer) in 6-cm-diameter dishes. After 3 weeks, colonies were counted, and pictures were taken.

Tumorigenicity assays. A total of 1×10^6 cells were resuspended in 50 μL Matrigel solution (BD Matrigel Basement Membrane Matrix HC; BD Biosciences) and immediately injected subcutaneously into 8-week-old female nude mice (BALB/cAnNCrl-nu BR). 2-D tumor sizes were measured once a week.

The tumor volume (mm^3) was calculated using the formula (length × width^2)/2.[21]

Results

Effect of HBx on cellular senescence of human primary cells. During immortalization, human cells differ from rodent cells in the regulation of telomere length[22,23] and cell cycle checkpoints.[24,25] Human cells must bypass two barriers to become immortalized: replicative senescence and crisis. Replicative senescence is characterized by an irreversible growth arrest but continued metabolic activity.[26] Crisis is characterized by widespread cell death.[26,27] By the introduction of hTERT, human primary cells avoid these two barriers and can become immortalized.[28–30]

It is possible that HBx contributes to the immortalization process of human primary cells, but not to the cellular transformation process. If so, it may facilitate cellular transformation indirectly by overcoming two crises, M1 and M2. To study whether this does facilitate cellular transformation, it is best to use human primary hepatocytes as HBV is a hepatotropic virus. However, human primary hepatocytes are almost impossible to obtain for such an experimental approach. HBx exhibits its transactivation function not only in hepatoma cell lines but also in various carcinoma and sarcoma cell lines. Under these situations, we addressed whether HBx contributes to the immortalization of human primary fibroblasts, BJ cells and TIG3 cells that have been well studied for cellular senescence and immortalization. We used hTERT-introduced BJ and TIG3 cells for positive controls of immortal cells.

The human primary fibroblasts, BJ cells and TIG3 cells were infected with the HBx-expression retroviruses and cultured in the presence of the selection drug, blastcidin S. The drug-resistant polyclonal cells were selected and characterized. Three different constructs of HBx were used to map the responsible domain: full-length HBx (HBx-wt), HBx-D1, which lacks the N-terminal negative regulatory domain, and HBx-D5, which lacks the coactivation domain (Fig. 1a). First we examined HBx expression in the primary human fibroblasts. We found that full-length HBx and HBx-D5 were highly but equally expressed, whereas expression of HBx-D1 was very weak in the blastcidin S-selected clones (Fig. 1b). We hypothesized that HBx expression may confer an immortal phenotype, which could contribute to cellular transformation and tumorigenesis, but we observed that the BJ cells expressing HBx proteins stopped dividing at PD 69.6 ± 0.9 (errors ± SD) (HBx-wt), PD 66.6 ± 1.6 (HBx-D5), PD 66.1 ± 1.4 (HBx-D1) and PD 60.5 ± 0.6 (control cells) (Fig. 1c). TIG3 cells, another human fibroblast, expressing HBx proteins stopped dividing at PD 77.2 ± 1.1 (HBx-wt), PD 75.1 ± 0.8 (HBx-D5), PD 75.1 ± 0.1 (HBx-D1) and PD 75.4 ± 0.2 (control cells) (Fig. 1d). Although a very minor extended lifespan (2–4 PD) was observed with HBx-wt-expressing primary human fibroblasts, the HBx protein could not elicit immortalization. We examined whether the effect of HBx on delay of cellular senescence was correlated with putative augmentation of telomerase activity in HBx-introduced BJ and TIG3 cells (Fig. 1e) as activation of the hTERT promoter was observed in hepatoma cell lines that were transiently cotransfected with the HBx expression vector and luciferase reporter vector of the hTERT promoter (S. Murakami *et al.* unpublished data, 2005). Telomerase activity in the extracts of cells expressing HBx-wt or HBx-D1 was slightly higher than that of cells expressing empty vector or HBx-D5 in both kinds of cells (Fig. 1e), but we failed to detect an increase in hTERT protein expression (data not shown). Therefore, the relevance of the weak augmentation of telomerase activity in the HBx-expressing primary cells remains unclear.

Effect of HBx on immortalized BJ-hTERT cells. Next, we addressed whether HBx facilitates the cellular transformation process
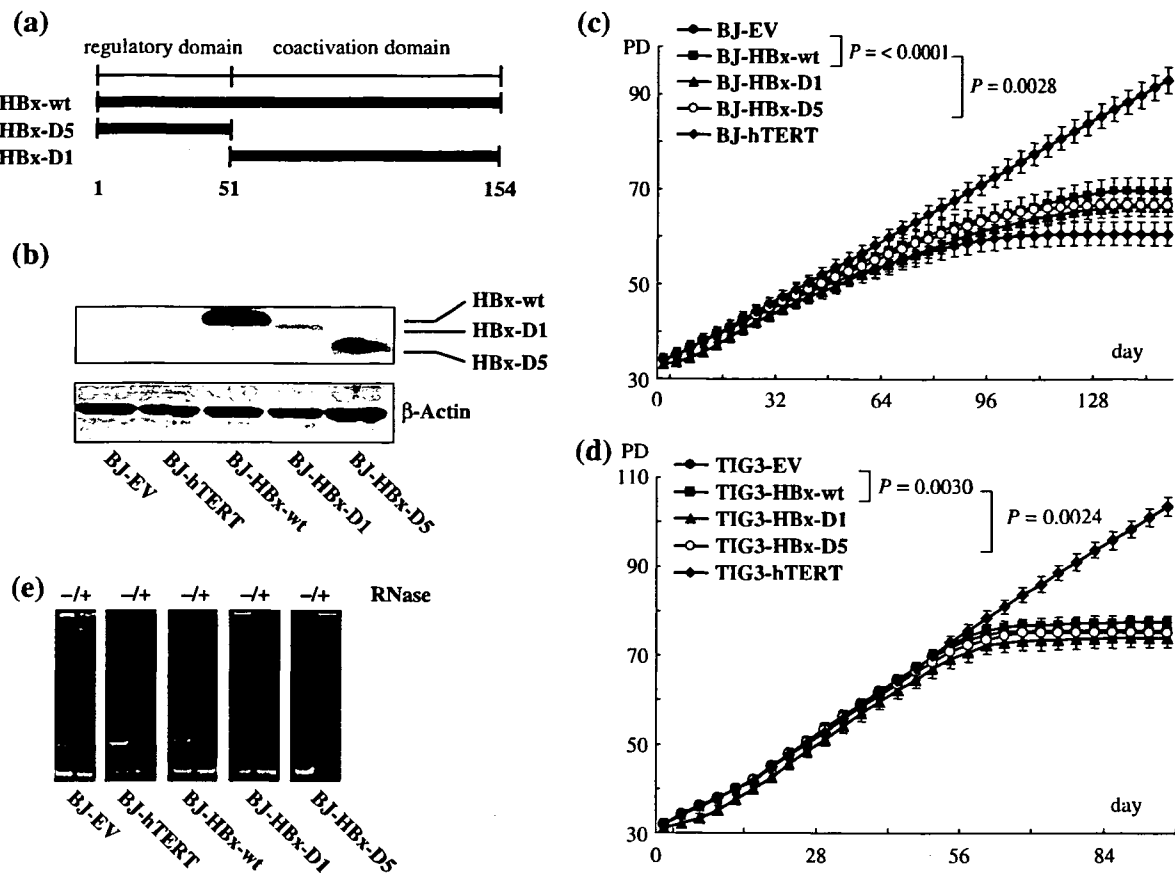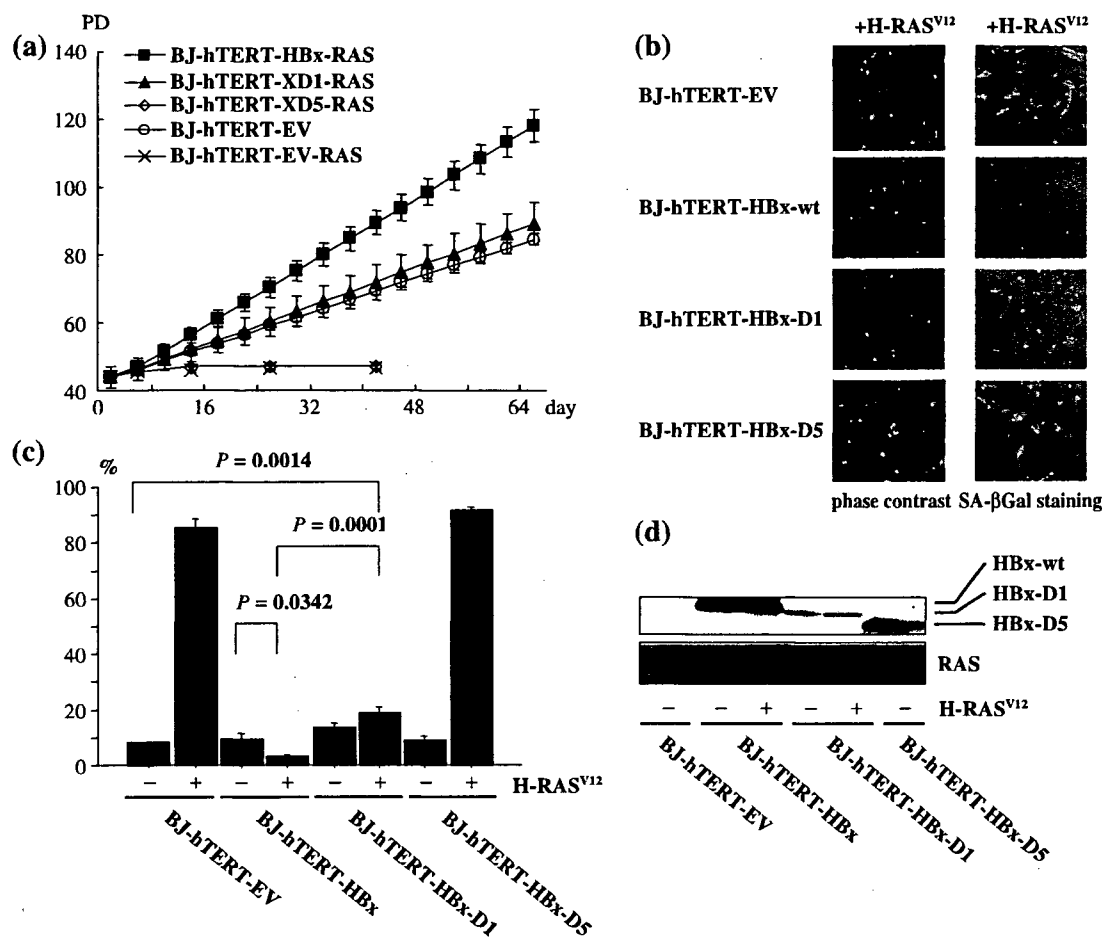
Fig. 1. Hepatitis B virus protein X (HBx) can not immortalize human primary cells, but weakly affects cellular senescence and telomerase activity. (a) Schematic representation of the HBx proteins.[5,8] The amino acids (aa) of full-length HBx (154 aa residues) and truncated HBx are shown. HBxD1 harbors the carboxy-terminal coactivation domain, spanning aa residues 51–154, whereas, HBxD5 harbors the amino-terminal negative regulatory domain, spanning aa residues 1–50. (b) Expression of HBx, HBx-D1 and HBx-D5 proteins in infected BJ cells. Total cell lysates of BJ cells infected with the empty vector (EV), human telomerase reverse transcriptase (hTERT), HBx, HBx-D1 and HBx-D5 expression retroviruses were fractionated by sodium dodecylsulfate–polyacrylamide gel electrophoresis and subjected to western blot analysis with anti-FLAG M2 antibody. (c) Effect of HBx on replicative senescence in BJ cells. BJ cells were infected with a control vector (filled circles) or hTERT (filled diamonds) and with a retrovirus encoding wild-type HBx (filled squares), HBx-D1 (filled triangles) or HBx-D5 (open circles). Cells infected with pBabe-puro- and pBabe-blast were selected with 1 μg/mL puromycin and 4 μg/mL blasticidin S, respectively. After 8 days of drug selection, triplicate samples of 1 × 10^5 cells were plated and grown under normal conditions (day 0). (d) Effect of HBx mutants on replicative senescence in TIG3 cells. Symbols are the same as in (c). (e) Telomerase activity in BJ cells as demonstrated by telomerase activity assay (TRAP). Total cell lysates (200 ng) prepared from BJ cells infected with control vector, hTERT, HBx, HBx-D1, and HBx-D5 were subjected to TRAP assay using a TRAPEZE kit (Intergen).

using human immortal cells. For this purpose, we used BJ-hTERT cells – these were BJ-derived cells immortalized by the introduction of hTERT, as characterized previously.[19] HBx-wt as well as its truncated mutants had no effect on cell proliferation, telomerase activity or cell transformation. Using the newly established TIG3-hTERT cells, we confirmed that the stable expression of HBx, XD1 or XD5 did not affect cell proliferation or cell transformation (data not shown). These results indicate the inability of HBx alone to transform these human immortalized cells.

Ability of HBx to overcome H-RAS^{V12}-induced senescence in BJ cells immortalized by hTERT Seeing as HBx did not exhibit the ability to immortalize primary human fibroblasts or to elicit transformation into hTERT-induced immortal primary human fibroblasts, we considered whether HBx functioned together with an oncogene and induced cell transformation. Senescence induced by active oncogene expression (OIS), such as oncogenic RAS, is one of the anticancer processes in which tumor suppressors and their related networks are involved, as demonstrated in vitro and recently also in vivo.[31,32] Overcoming OIS is critical for

cellular transformation in vitro and cancerous cell proliferation in vivo.[31] Therefore, we addressed whether HBx has a collaborating role in transforming cells in the presence of oncogenic RAS or in overcoming RAS-induced senescence.

To examine the effect of HBx on RAS-induced senescence-like growth arrest, we introduced H-RAS^{V12} into BJ-hTERT, BJ-hTERT-HBx-wt, BJ-hTERT-HBx-D1 and BJ-hTERT-HBx-D5 cells using a retrovirus (Fig. 2d). BJ-hTERT cells expressing H-RAS^{V12} stopped proliferating within several days of RAS introduction. In contrast, BJ-hTERT cells expressing both H-RAS^{V12} and HBx-wt (BJ-hTERT + H-RAS^{V12} + HBx-wt) continued to proliferate to more than 80 PD (Fig. 2a). Although HBx-D1 also demonstrated the ability to overcome active RAS-induced senescence, HBx-D5 failed to overcome OIS (Fig. 2a). We also found that the growth rate of BJ-hTERT + H-RAS^{V12} + HBx-wt cells was much higher than that of BJ-hTERT + H-RAS^{V12} + HBx-D1 cells, probably reflecting the fact that some portion of the latter cells were positive for SA-β-gal (Fig. 2b,c). Consistent with this result, cells staining positive for SA-β-gal were significantly fewer in BJ-hTERT +

(a)

PD

140

- BJ-hTERT-HBx-RAS
- BJ-hTERT-XD1-RAS
- BJ-hTERT-XD5-RAS
- BJ-hTERT-EV
- BJ-hTERT-EV-RAS

120

100

80

60

40

0   16   32   48   64 day

(b)

+H-RAS^{V12} +H-RAS^{V12}

BJ-hTERT-EV

BJ-hTERT-HBx-wt

BJ-hTERT-HBx-D1

BJ-hTERT-HBx-D5

phase contrast SA-β-Gal staining

(c)

%

$P = 0.0014$

100

80

$P = 0.0001$

60

$P = 0.0342$

40

20

0

− + − + − + − +   H-RAS^{V12}

BJ-hTERT-EV   BJ-hTERT-HBx   BJ-hTERT-HBx-D1   BJ-hTERT-HBx-D5

(d)

HBx-wt
HBx-D1
HBx-D5

RAS

− − + − + −   H-RAS^{V12}

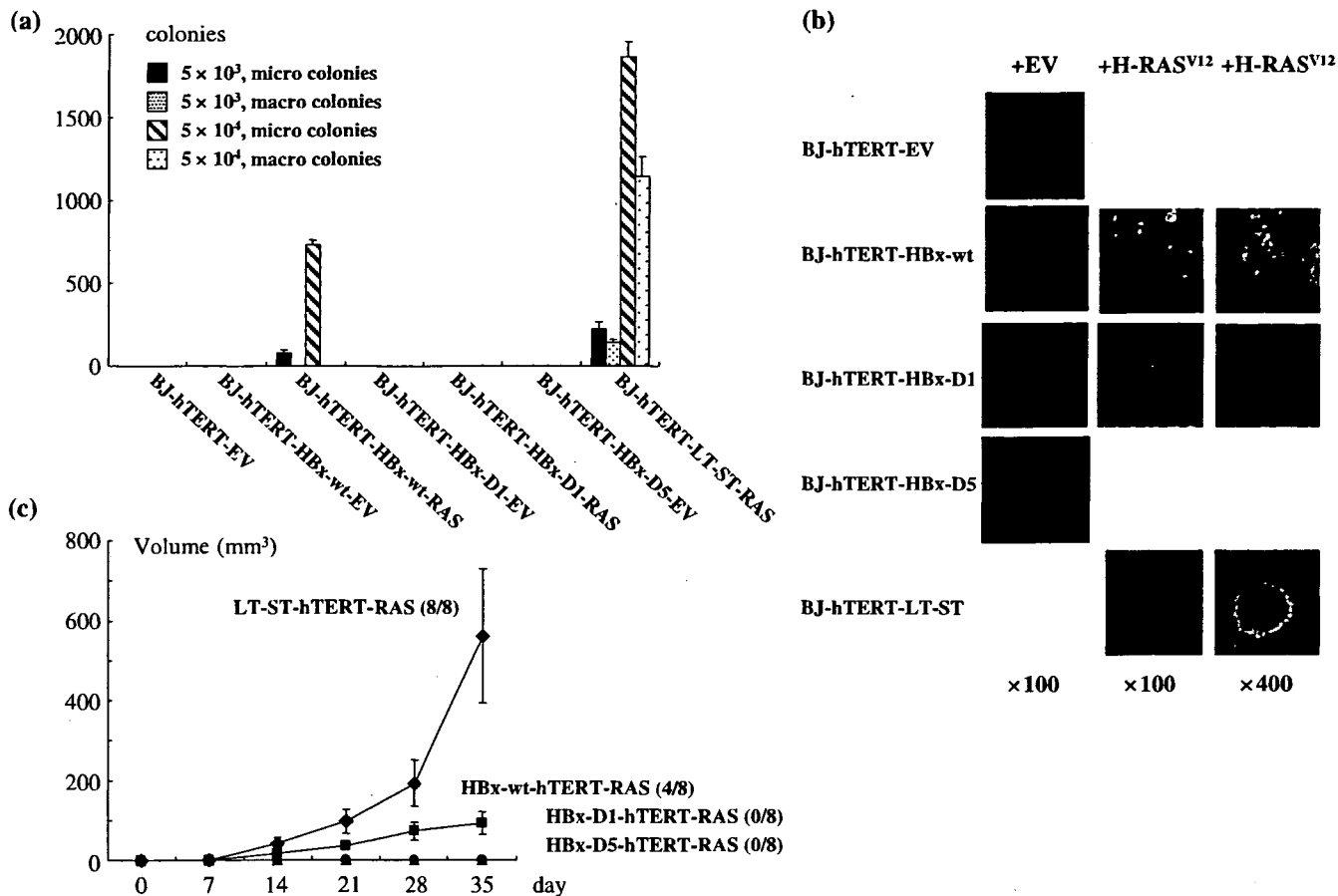BJ-hTERT-EV   BJ-hTERT-HBx   BJ-hTERT-HBx-D1   BJ-hTERT-HBx-D5

Fig. 2. Hepatitis B virus protein X (HBx) can overcome H-RAS^{V12}-induced cellular senescence of human immortalized cells. (a) Effect of HBx on H-RAS^{V12} induced senescence. BJ-human telomerase reverse transcriptase (hTERT) cells (open circles) and H-RAS^{V12}-induced BJ-hTERT-HBx-wt (filled squares), BJ-hTERT-HBx-D1 (filled triangles), BJ-hTERT-HBx-D5 (filled diamonds) cells and BJ-hTERT-empty vector (EV) (cross) are shown. After 10 days of drug selection at population doubling (PD) 42, triplicate samples of 1×10^5 cells were plated and grown under normal conditions (day 0). (b) HBx overcomes H-RAS^{V12}-induced senescence of human immortalized cells. H-RAS^{V12} and EV, full-length or truncated forms of HBx were introduced into BJ-hTERT cells. Left panel shows photographs 10 days after infection of the H-RAS^{V12}-expression retrovirus. Right panels show senescence-associated β-galactosidase (SA-β-Gal) staining 10 days after infection. (c) The percentage of cells positive for SA-β-Gal was determined in BJ cells stably expressing HBx-wt, HBx-D1, HBx-D5 or empty vector, with or without H-RAS^{V12} on day 9 after infection. Bars = mean ± SD. (d) Western blot analysis of RAS-induced cells. Total cell lysates from BJ-hTERT cells stably expressing HBx-wt, HBx-D1, HBx-D5 or EV together with or without H-RAS^{V12} were prepared and fractionated by sodium dodecylsulfate–polyacrylamide gel electrophoresis, then subjected to western blot analysis. HBx-wt, HBx-D1 and HBx-D5 were detected with anti-FLAG M2 antibody. RAS protein was detected with anti-RAS antibody.

H-RAS^{V12} + HBx-wt than in BJ-hTERT + H-RAS^{V12} + HBx-D1 (Fig. 2c). These results indicate that HBx-wt has the ability to overcome RAS-induced senescence. HBx-D1, the coactivator domain of HBx, seems to be indispensable and sufficient for overcoming RAS-induced senescence analyzed by the PD analysis, although HBx-D1 did not show the same ability as HBx-wt. The incomplete ability of HBx-D1 may be due to the low expression of HBx-D1 in the blasticidin S-selected clones in BJ-hTERT cells, as observed with the BJ cells (see Discussion).

HBx protein is required for anchorage-independent growth and tumor formation in nude mouse in response to H-RAS^{V12}. HBx can overcome RAS-induced senescence (examined by the PD analysis) and can indicate that HBx and RAS can induce cell transformation. Therefore, we examined whether BJ-hTERT + H-RAS^{V12} + HBx-wt and BJ-hTERT + H-RAS^{V12} + HBx-D1 cells can form colonies in soft agar. We found that BJ-hTERT + H-RAS^{V12} + HBx-wt cells showed cell number-dependent formation of colonies, which were much smaller size than those of control

cells, BJ-hTERT + H-RAS^{V12} + SV40 LT + ST$^{(20,33)}$ (Fig. 3a,b). In contrast, BJ-hTERT + H-RAS^{V12} + HBx-D1 cells could not form colonies in soft agar (Fig. 3a), although these cells overcame RAS-induced senescence. This result strongly suggests that HBx-D1 is not equivalent to HBx-wt in its ability to make colonies in soft agar.

Next we tested the tumor-forming ability of BJ-hTERT + H-RAS^{V12} + HBx-wt or HBx-D1 cells in nude mice. BJ-hTERT + H-RAS^{V12} + HBx-wt cells were found to form tumors in four of eight mice, although these tumors grew much more slowly and were much smaller than those formed by BJ-hTERT + H-RAS^{V12} + SV40 LT + ST cells (eight of eight animals) (Fig. 3c). In contrast, BJ-hTERT + H-RAS^{V12} + HBx-D1 cells did not generate tumors in nude mice (Fig. 3c), consistent with the results of the soft-agar assay. These results indicate that HBx contributes to cellular transformation by collaborating with active RAS in human immortalized cells. To our knowledge, this is the first report showing that HBx plays a critical role in

(a)

colonies

- ■ 5 × 10³, micro colonies
- ▨ 5 × 10³, macro colonies
- ◩ 5 × 10⁴, micro colonies
- ⬚ 5 × 10⁴, macro colonies

(y-axis: 2000, 1500, 1000, 500, 0)

(x-axis labels, diagonal): BJ-hTERT-EV, BJ-hTERT-HBx-wt-EV, BJ-hTERT-HBx-wt-RAS, BJ-hTERT-HBx-D1-EV, BJ-hTERT-HBx-D1-RAS, BJ-hTERT-HBx-D5-EV, BJ-hTERT-LT-ST-RAS

(b)

+EV   +H-RAS^V12   +H-RAS^V12

BJ-hTERT-EV

BJ-hTERT-HBx-wt

BJ-hTERT-HBx-D1

BJ-hTERT-HBx-D5

BJ-hTERT-LT-ST

×100   ×100   ×400

(c)

Volume (mm³)

(y-axis: 800, 600, 400, 200, 0)

LT-ST-hTERT-RAS (8/8)

HBx-wt-hTERT-RAS (4/8)
HBx-D1-hTERT-RAS (0/8)
HBx-D5-hTERT-RAS (0/8)

(x-axis: 0, 7, 14, 21, 28, 35 day)

Fig. 3 (a,b) Anchorage-independent growth in soft agar and (c) tumorigenicity and tumor-forming ability in nude mice of cells expressing hepatitis B virus X protein (HBx) and H-RAS^V12. (a) Soft-agar assays were carried out as described in Materials and Methods.[19] After 3 weeks, colonies were counted and pictures were taken. The colony-forming ability of BJ-human telomerase reverse transcriptase (hTERT) cells stably expressing wild-type or truncated HBx with or without H-RAS^V12 is indicated at the bottom. H-RAS^V12-introduced BJ-hTERT-LT-ST cells were the positive control. (b) Morphology of colonies in the soft-agar assay. Colonies were photographed 21 days after seeding. (c) Tumor formation in nude mice was carried out as described previously in Materials and Methods.[19,21] Tumor sizes were measured once a week. Each point on the graph represents the average volume of tumors. BJ-hTERT-LT-ST-RAS (filled diamonds), BJ-hTERT-HBx-RAS (filled squares), BJ-hTERT-HBx-D1 (filled circles), and BJ-hTERT (filled triangles) cells are shown. Error bars indicate the mean ± SD for each time point.

cellular transformation, collaborating with active RAS in human immortalized cells.

Effects of HBx on p16 and p21 expression and the ability of HBx to overcome RAS-induced senescence. Overexpression of RAS causes oncogene-induced premature senescence in normal human fibroblasts (Fig. 4c) and hTERT-immortalized human fibroblasts (Fig. 2a), but RAS failed to induce premature senescence in HBx-wt- or HBx-D1-introduced BJ-hTERT cells (Fig. 2a). We next examined the effect of stable expression of HBx in BJ cells with or without expression of hTERT, as interference with both the p53 and pRb pathways is necessary to avoid RAS-induced cellular senescence, in which p16 and p21 are the critical downstream effectors of pRb and p53, respectively. Expression of p16 and p21 was upregulated in HBx-wt- or HBx-D1-introduced BJ-hTERT cells; however, HBx-D5 has no ability to induce the expression of these genes. The presence of H-RAS^V12 resulted in downregulation of the augmented expression of p16 and p21 in HBx-wt- or HBx-D1-introduced BJ cells and BJ-hTERT cells (Fig. 4a,b). These results suggest that HBx can suppress expression of p53, p16 and p21 in H-RAS^V12-introduced cells, contributing to overcoming RAS-induced senescence. Next we examined whether HBx-wt and H-RAS^V12 not immortalized

by hTERT were sufficient for cellular transformation. We introduced H-RAS^V12 into BJ-HBx-wt, BJ-HBx-D1 and BJ-HBx-D5 cells and analyzed them by PD analysis and soft-agar colony assay. In the PD analysis, H-RAS^V12-introduced BJ-HBx-wt and BJ-HBx-D1 cells did overcome RAS-induced cellular senescence but stopped cell division at PD 62, which is approximately the cellular senescence of BJ cells (Figs 1c,4c), whereas H-RAS^V12-introduced BJ-HBx-D5 did not overcome senescence and stopped cell division. These results suggest that HBx can overcome RAS-induced senescence but can not immortalize the cells (Fig. 4c). In the soft-agar colony formation assay, BJ-HBx-wt-H-RAS^V12 and BJ-HBx-D1-H-RAS^V12 could but BJ-HBx-D5-H-RAS^V12 could not form very tiny colonies, suggesting that HBx-wt and H-RAS^V12 in the absence of hTERT may enable the cells to proliferate in an anchorage-independent manner (data not shown).

As HBx-D1, which was very weakly expressed, exhibited almost the same ability as HBx-wt to upregulate the tumor suppressor genes and to overcome RAS-induced senescence in these cells, we wondered whether HBx-D1 missing the N-terminal domain may have some negative effect on cell proliferation. Because the transient expression level of HBx-D1 in BJ cells was similar to those in HepG2 cells, as reported previously
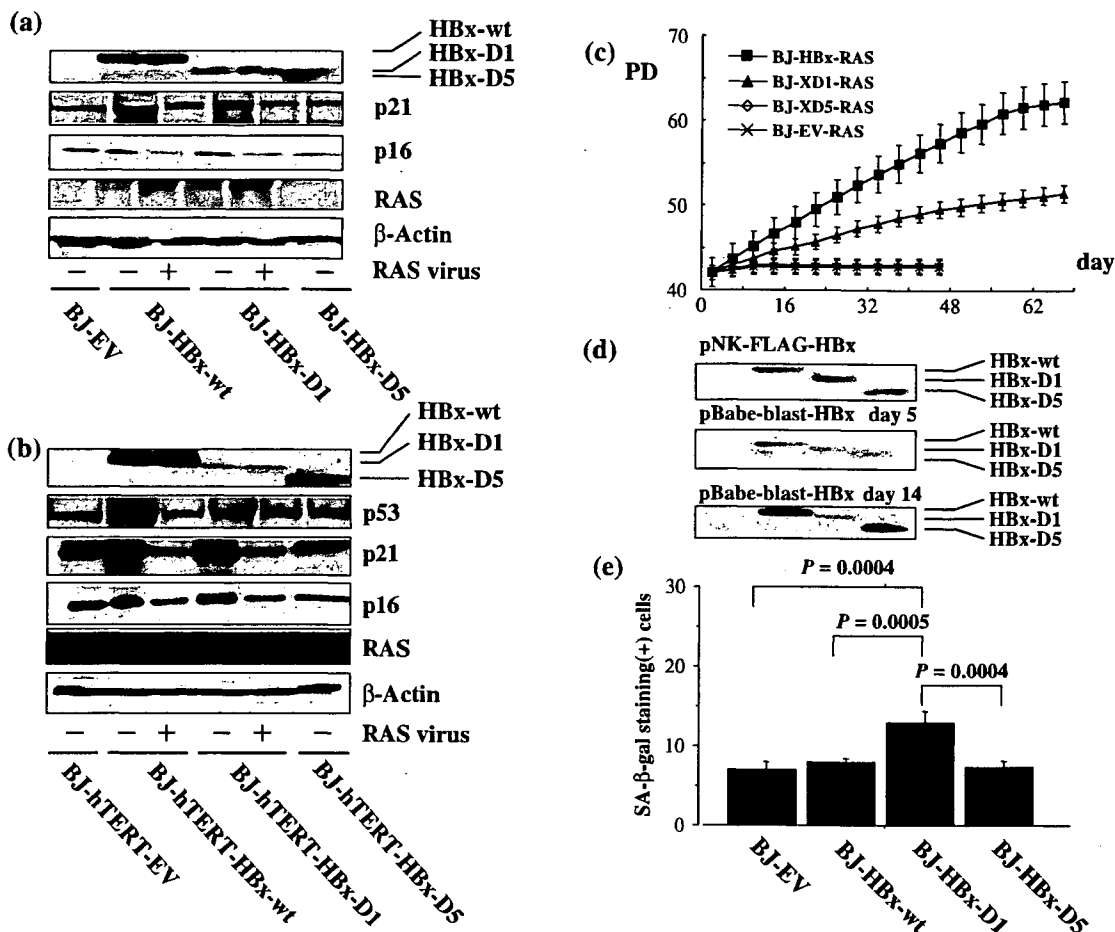
Fig. 4. Effect of hepatitis B virus X protein (HBx) on p16 and p21 expression and the ability of HBx to overcome H-RAS^{V12}-induced cellular senescence of human normal cells. Total cell lysates from BJ-human normal telomerase reverse transcriptase (hTERT) cells stably expressing HBx-wt, HBx-D1, HBx-D5 or empty vector together with or without H-RAS^{V12} were prepared, and fractionated by sodium dodecylsulfate–polyacrylamide gel electrophoresis (SDS-PAGE), then subjected to western blot analysis. Expression of (a) p16 and p21 proteins and (b) p53, p16 and p21 proteins. (c) Effect of HBx on H-RAS^{V12}-induced senescence. Population doublings (PD) of H-RAS^{V12}-induced BJ-HBx-wt (filled squares), BJ-HBx-D1 (filled triangles), BJ-HBx-D5 (open diamonds) and BJ-EV (cross) cells are shown. After 10 days of drug selection, at PD 44, triplicate samples of 1×10^5 cells were plated and grown under normal conditions (day 0). (d) Expression of HBx, HBx-D1 and HBx-D5 proteins in infected BJ cells. Total cell lysates of BJ cells transfected with mammalian expression plasmids of FLAG-HBx-wt, FLAG-HBx-D1 and FLAG-HBx-D5 were fractionated by SDS-PAGE and subjected to western blot analysis with anti-FLAG M2 antibody (upper panel). Total cell lysates of BJ cells infected with the empty vector (EV), HBx-wt, HBx-D1 and HBx-D5 expression retroviruses were fractionated by SDS-PAGE and subjected to western blot analysis with anti-FLAG M2 antibody (middle and bottom panel). (e) The percentage of cells positive for senescence-associated β-galactosidase (SA-β-Gal) was determined in BJ cells stably expressing HBx-wt, HBx-D1, HBx-D5 or empty vector (EV) on day 40 after infection. Bars = mean ± SD.

(Fig. 4d),[8] it was not due to the construct design of the vector. The expression of HBx-D1 was slightly lower than those of HBx-wt and HBx-D5 on day 5 after selection, much lower on day 10 after selection (data not shown). On day 14 after selection, the expression of HBx-D1 reached the lowest level, and after day 14 that expression level was kept (Figs 1b,4d). HBx-D1-introduced BJ cells grew slower than HBx-wt- or HBx-D5-introduced BJ cells (data not shown) and contained more SA-β-Gal-positive cells during proliferation (Fig. 4e). These results suggest that cells expressing lower levels of HBx-D1 proliferated more than cells expressing higher levels of HBx-D1, due to some toxic or antiproliferative effect of the coactivation domain of HBx in the human primary cells (see Discussion).

Important region of HBx for overcoming cellular senescence and anchorage-independent growth. As HBx exhibited the ability to overcome active RAS-induced senescence, we next tried to identify the critical regions of HBx for overcoming cellular

senescence. BJ-hTERT cells were infected with retroviruses expressing one of the clustered alanine-substituted mutants covering all parts of HBx,[34] and a series of cell clones stably expressing these HBx-cm mutants, BJ-hTERT-HBx-cm, was established (Fig. 5). H-RAS^{V12} was then introduced into BJ-hTERT-HBx-cm1 to BJ-hTERT-HBx-cm21 cells and cell proliferation was examined. The regions covering HBx-cm8 to HBx-cm10, and those covering HBx-cm19 to HBx-cm21 were found to be not critical for overcoming active RAS-induced senescence and anchorage-independent growth as the BJ-hTERT-RAS clones expressing these HBx-cm mutants proliferated and formed colonies in soft agar, similar to BJ-hTERT-HBx-wt-H-RAS^{V12} cells. The BJ-hTERT-RAS clones expressing HBx-cm1 to HBx-cm7, and those expressing HBx-cm14 to HBx-cm16, were like BJ-hTERT-HBx-D1-RAS, which can grow but at a much reduced rate compared with BJ-hTERT-HBx-RAS cells. The HBx regions covering HBx-cm11 to HBx-cm13, HBx-cm17